공학박사 학위논문

Temperature Responsive Drug Delivery Systems by Combining Nanoparticles and Flexible Devices

나노입자와 유연소자를 활용한

온도 민감성

약물전달시스템 구현

2017년 8월

서울대학교 대학원

화학생물공학부

송 창 영

Abstract

Temperature Responsive Drug Delivery Systems by Combining Nanoparticles and Flexible Devices

Changyeong Song

School of Chemical and Biological Engineering

The Graduate School

Seoul National University

Recently, nanoparticles have been investigated for their applications to biomedical areas including diagnosis, therapy and theranostics.

Controlled drug release systems with internal/external stimuli can provide the effective therapeutic functions on targeted region. Among stimuli-responsive drug delivery, temperature-responsive drug delivery enables on/off, step-wised, and multi-stage drug delivery with controlled heating. With integration of flexible devices, temperature-responsive drug delivery can make considerable progress such as precise control of temperature, multi-stage delivery, and wireless control system.

Firstly, temperature-responsive microneedles were fabricated with introducing phase change material (PCM) to the conventional microneedle system. To utilize phase change material as drug carriers, I successfully synthesized phase change nanoparticles (PCNs) with probe-ultrasonicating process. Using different PCMs, I could control the temperature of drug releasing at 40 and 45 oC, respectively. The phase change nanoparticles (PCNs) could load the type 2 diabetes drug (metformin) and only release the drugs when they are heated above melting temperatures. By integrating with three channel heaters and temperature sensors, microneedles enable multi-stage drug delivery upto six releasing amounts for diabetes treatment.

Secondly, theranostic nanoparticles were developed by coating of

temperature-responsive polymers with photo- and chemo-drugs for colon cancer treatment. By integrating lasers with endoscope system, I could overcome penetration depth problem of lasers. With irradiation of near-infrared (NIR) laser, Au nanorods generate heat, which can function as photothermal therapy and activate temperature-responsive delivery of doxorubicin. Also, photodynamic dyes on mesoporous silica shells can act as both imaging and therapeutic agents with red laser. These combined therapies (photothermal, photodynamic, and chemotherapy) made synergistic effect of colon cancer treatment in in-vitro and in-vivo experiments. The nanoparticles can actively deliver to colon cancer cells by conjugated antibodies and selectively treat cancer cells with irradiation of red/NIR lasers, which reduces side effects of cancer therapy.

Keywords: Nanoparticle, Temperature responsive, Flexible devices, Drug delivery, Microneedles, Nanobio technology

Student Number: 2011-22920

Contents

List of Figures

Chapter 1. Introduction:

Device-assisted Transdermal Drug Delivery

1.1 Introduction

The growing demand for patient-friendly therapies has led to the development of transdermal drug delivery that has several advantages over conventional drug delivery methods such as oral and injectable delivery. For instance, it enables sustained and controlled drug release, and is virtually non-invasive and painless, promoting patients' compliance and convenience.[1] In particular, the transdermal route is a good alternative to needle injection or oral intake of medication. Such advantages of transdermal delivery are exemplified by the commercial success of scopolamine and nicotine patches in the 1970s and 1980s. However, transdermal drug delivery has several drawbacks that limit its efficiency. For example, outermost stratum corneum layer in the skin

works as a major diffusion barrier making the vast majority of candidate drugs unsuitable for transdermal delivery. Inter- and intra-patient differences also may cause variations in drug delivery rates as well as fluctuation in pharmacokinetic profiles.[2]

Decades of research has yielded considerable success in overcoming such limitations and maximizing the efficiency of transdermal drug delivery. Furthermore, transdermal delivery is set to adopt an advanced paradigm of device-assisted personalized therapy[3-5] where the precise control of the amount and duration of a drug dose in response to the patient's physiological condition is a key to maximizing the therapeutic efficacy. The controlled and on-demand administration of a drug tailored to the needs of each patient requires extensive innovation. Wearable devices may be a viable and useful strategy because they can collect an assortment of physiological,[6-15] electrophysiological,[16-21] and biochemical[22-27] cues, and thereby, facilitate drug delivery via energetic actuations.

In this chapter, I summarize the major breakthroughs of four generations of transdermal drug delivery strategies, providing the reader with the detailed advantages and challenges of each generation. In accordance with a growing interest in controlled drug release for

personalized medical treatment, I also emphasize the recent progress on wearable devices that support device-assisted transdermal drug delivery. This chapter concludes with case presentations to demonstrate the wearable biosensors and advanced transdermal delivery schemes that are seamlessly integrated. Thereby, I hope to present a novel potential protocol and foundation for the next generation of personalized therapy.

1.2 Overview of device-assisted transdermal drug delivery systems

Personalized therapy is distinct from conventional medical treatments by its ability to adjust the treatment to each individual's pathophysiological conditions.[28] Therefore, the establishment of personalized therapy requires systematic control of the administered dose based on an accurate real-time observation of the patient's physiological parameters to determine the disease status and drug efficacy. In response to the increasing need for personalized treatment, the advanced transdermal delivery system empowered by soft bioelectronics has been spotlighted as a strategy for the next generation drug delivery method.

The rapid advances in soft and ultrathin devices in wearable forms have enabled the seamless integration of bioelectronic devices in a skin-mounted patch domain with unprecedented functionalities (**Figure 1.1**).[29-31] Specifically, sensors accurately measure the physiological,[6-15] electrophysiological,[16-21] and biochemical[22-27] signals; actuators transfer energy to the drug-laden patch in a controlled manner, and the sensors subsequently gather information on the therapeutic efficacy of

the drug. The synergetic performance of wearable devices and drug-delivering patches following a completed feedback loop provides a novel platform for personalized therapy (**Figure 1.2**).

To maximize the performance of device-assisted transdermal drug delivery, a conformal contact between the device and the skin stemming from the stretchability and flexibility of the device is crucial. The soft nature and deformability of the system minimize the local detachment and microscopic spaces between the device and the skin due to the curvilinear morphology of the skin and bodily movements.[16] Conformal integration to the skin also promotes precise measurements of the biological signals with minimal motion-induced noise, enhancing the accuracy of wearable sensors monitoring physiological (*e.g.,* blood pressure, strain, and temperature),[6-15] electrophysiological (*e.g.,* electrocardiogram and electroencephalogram),[16-21] and biochemical (*e.g.,* pH, blood glucose, and oxygen levels)[22-27] signals from the skin. Based on the collected information, a co-integrated actuator controls the drug diffusion rate. This process is also enhanced by the conformal contact because a stable interface between the patch and the skin ensures homogeneous and efficient energy transfer, and provides a uniform drug release profile throughout the entire patch area.[32,33]

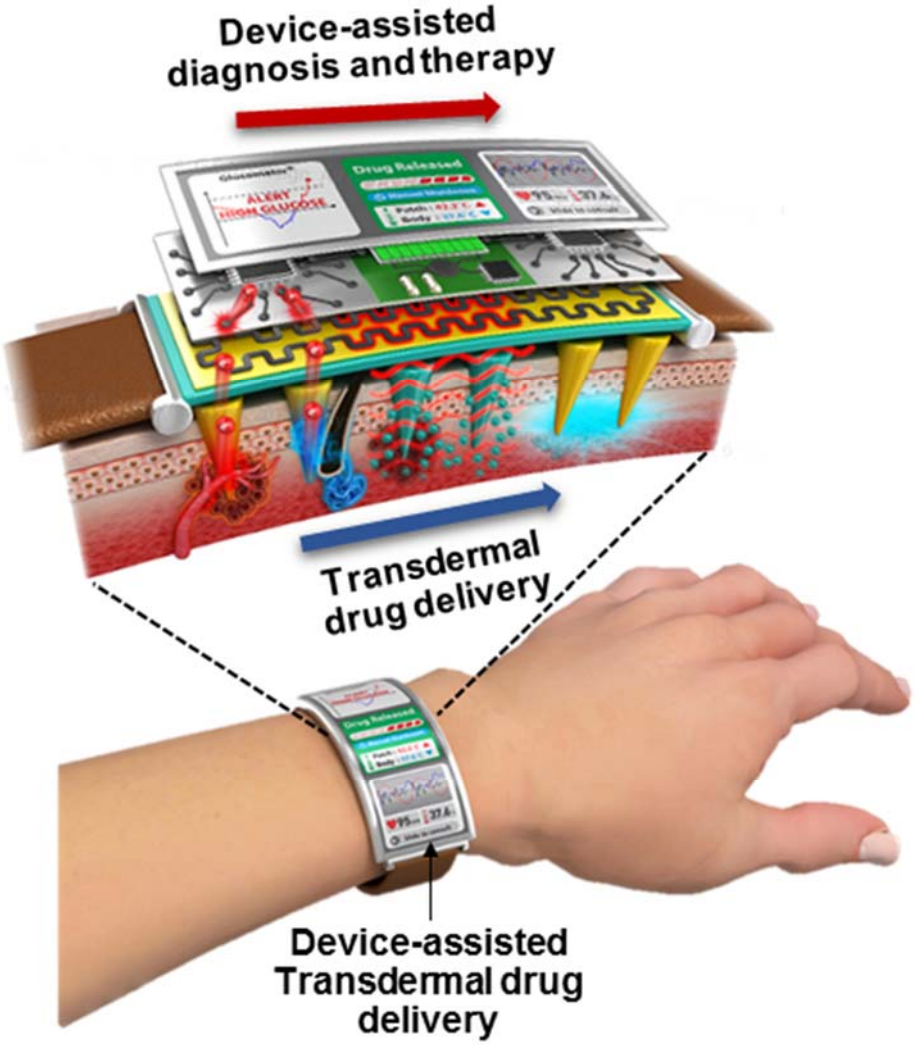

Figure 1.1. Schematic illustration of the device-assisted transdermal drug delivery for patient-customized skin-based therapy.

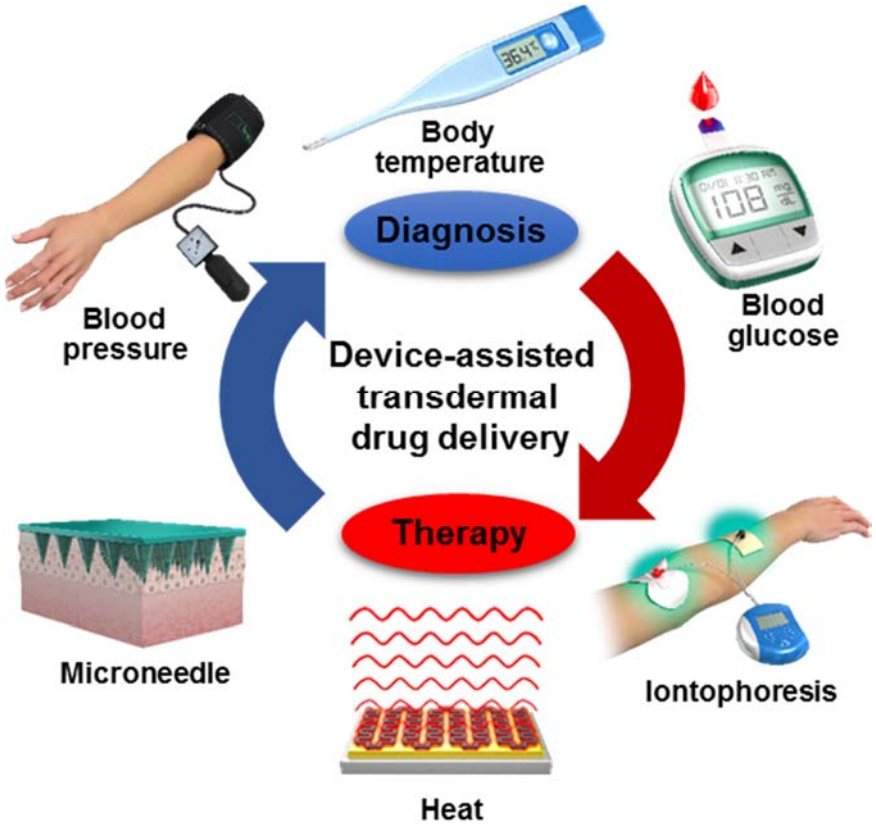

Figure 1.2. The wearable device system conducts real-time monitoring of vital signs and actuates transdermal drug delivery according to individual health condition.

1.3 Advancement of transdermal drug delivery systems

Among the anatomical layers and appendageal structures of the skin (**Figure 1.3**), the epidermis and its outermost stratum corneum layer are the most challenging barriers to transdermal delivery.[34,35] The brick-and-mortar assembly of keratinocytes and intercellular lipids renders the epidermis impregnable to most foreign materials. Therefore, a cursory observation of transdermal delivery can regard it as a counterintuitive strategy for delivering a drug systematically. However, a detailed analysis reveals that transdermal delivery provides a number of advantages over oral intake or hypodermic injections. Compared with oral delivery, transdermal delivery requires a lower dosage and has fewer side effects because transdermal diffusion circumvents the digestion and first-pass metabolism of the active drug in the gastrointestinal tract and liver.[36] Moreover, transdermal delivery is less painful, minimally invasive, and convenient to patients so that the compliance with drug administration increases to a great extent. Because such advantages offset the drawbacks of transdermal delivery, studies continue to develop reliable delivery systems and broaden the library of applicable candidate drugs. Novel designs of transdermal patches to increase the skin

penetration of drugs have been widely investigated, and major breakthroughs have been observed as the evolving generations of transdermal delivery systems.

The research on the first generation of transdermal drug delivery systems focused on tailoring the physicochemical properties of chemical drugs. Drugs for transdermal delivery are either selected or modified to have a high partition coefficient and a low molecular weight for facile diffusion through the skin barrier (**Figure 1.4a**). The second-generation research focused on improving the skin permeability of drugs using chemical enhancers and stimulators through external driving forces (**Figure 1.4b**). Chemical enhancers[37,38] and emulsion/nano-carriers[39-42] solubilize the drugs and facilitate their easy penetration into the skin. External actuation using heat,[43] electricity,[44] or noncavitational ultrasound[45] also facilitates drug transportation. The third-generation research adopted methods that cause microscopic destruction of epidermis to facilitate the delivery of drugs. Radiofrequency (RF) ablation,[46] ultrasound,[47] and lasers[48,49] disrupt the stratum corneum temporarily and enhance drug penetration through the weakened barrier. Microneedles are another approach of microinvasive transdermal delivery with vastly diverse drug candidates.[50-53] The microneedles

create micrometer-sized porations in epidermis, which serve as an unobstructed pathway for incoming drugs (**Figure 1.4c**). Since the size of the microneedles leaves the dermal and hypodermal layers untouched, the microneedle is considered virtually painless and minimally invasive.

While breakthroughs in transdermal delivery in previous generations have focused on maximizing the efficiency of drug delivery, the recent growth in personalized medicine requires a new generation of the drug delivery system aimed at controlled and feedback-induced transdermal release of drugs. Wearable devices consisting of sensors and actuators are expected to meet such needs.[28,54,55] Indeed, novel materials design and device fabrication have spurred the innovation in wearable devices for biomedical application, providing a new opportunity in personalized healthcare [56]. By precisely monitoring the key indicators of disease treatment and potential side effects of the delivered drugs, decisions can be rapidly made on the appropriate amount of drug to be delivered. The external energy stimulates and controls state-of-the-art transdermal delivery systems. Device-assisted transdermal delivery, an ensemble of soft bioelectronics and a transdermal drug delivery system, simultaneously controls the release of drugs and monitors the alteration of the physiological states by the drug (**Figure 1.4d**). The cycle of

prognosis, actuated drug release, and follow-up diagnosis constitute a feedback loop that provides patients with a precise and personally customized medical treatment.

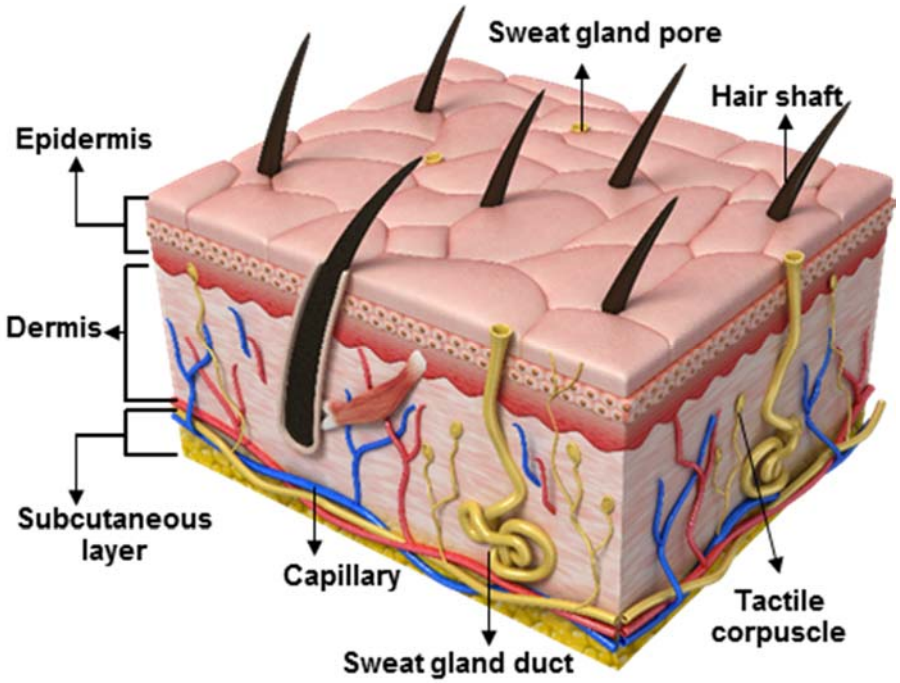

Figure 1.3. Schematic illustration of human skin.

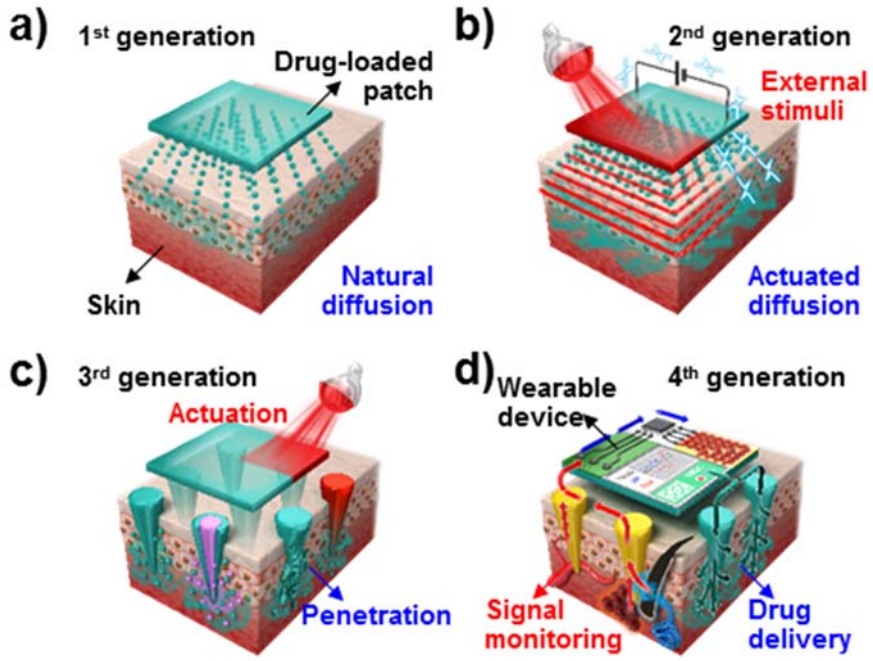

Figure 1.4. Schematic illustrations of advancement of transdermal drug delivery. (a) First generation transdermal drug delivery technology via natural diffusion of drugs. (b) Second generation transdermal drug delivery technology for actuated drug delivery via external stimulation. (c) Third generation transdermal drug delivery technology for enhanced drug transport via microneedle-mediated destruction of skin layer and various functionalities accompanying microneedles. (d) Fourth

generation transdermal drug delivery technology for patient-customized therapy with the assistance of wearable devices.

1.3.1 First-generation transdermal drug delivery technology

Transdermal drug delivery is an attractive drug delivery option because it offers several advantages. Firstly, the short distance of several dermal layers to the vasculature provides a faster route to the bloodstream than that of the convoluted gastrointestinal tract.[1] The transdermal shortcut also enhances bioavailability and reduces the drug dose because the delivered drug avoids the extensive first-pass metabolism and degradation in liver. Secondly, patients comply more easily with drug administration via transdermal delivery because a patch is easy to use, painless, and non-invasive. A long-lasting patch that provides sustained drug release for up to several days is convenient for patients, and its non-invasiveness allows repeated drug application over the same part of the body. Freedom from pain, particularly compared to needle-based injections, increases the popularity and acceptance of the transdermal delivery.

The first generation of simple transdermal patches emerged during the early 1970s. Following the first approval from the U.S. Food and Drug Administration (FDA) for the use of scopolamine patch for motion sickness, approximately 19 patches including nicotine, menthol, and estradiol are commercially available to date.[57] However, the number of

drugs that are suitable for patch formulation is severely limited because of the physiological barrier of the epidermis. The vast majority of the first generation transdermal drugs are highly lipophilic with partition coefficients greater than 10^4, small particle sizes, and molecular weights no more than 400 Da.[58]

1.3.2 Second-generation transdermal drug delivery technology

The second-generation transdermal delivery strategies seek to maximize the drug permeability of skin using chemical enhancers or external energy sources to stimulate delivery. Chemical enhancers facilitate the penetration of drugs by interacting with the proteins in skin and by increasing the drug solubility.[1] Presently, more benign chemical enhancers (*e.g.*, fatty acids, urea, and pyrrolidone) compared to skin-irritating or dermally toxic chemicals such as dimethyl sulfoxide (DMSO), dimethylformamide (DMF), and oxazolidinone are available to use.[59]

Emulsions comprise a major transdermal delivery strategy because they solubilize a wide range of both lipophilic and hydrophilic drugs in a transdermal formulation.[60] The absorption profile of an emulsion is determined based on the droplet size, composition, and surface charge. Particularly, reducing the size of vehicle particles to micrometer or nanometer level has been a popular strategy because smaller droplets can easily permeate the tight junctions of the skin barrier.[61,62] Recently, nanomaterials have been studied as potential systems for the delivery and controlled release of various drugs (*e.g.*, nucleic acid, antibacterial, and cancer drugs).[63-67] For example, drug-loaded nanoparticles (NPs)

effectively overcome the epidermal barrier and deliver an encapsulated cocktail of anti-inflammatory siRNAs and capsaicin. In contrast, the therapeutic agents in solution were obstructed from penetrating the stratum corneum (**Figure 1.5a**).[68] The efficiency of drug delivery control can be enhanced by using physicochemical-stimuli-responsive nano-sized vehicles.[69] One example is the temperature-responsive nanogel that significantly increases drug release as the temperature elevates from room to skin surface temperature (**Figure 1.5b**).[70] The pH-responsive release of antibacterial drugs into the skin in response to the acidic microenvironment induced by a virulent biofilm is another approach for the stimuli-responsive drug release (**Figure 1.5c**).[71]

Stimuli-responsive nano-vehicles are incorporated into patches to yield a synergetic efficacy in transdermal delivery. External stimuli (*e.g.*, light, mechanical force, and magnetic field) promote not only a higher rate of drug absorption but also a facile initiation and termination of drug administration.[63,72,73] Visible light can trigger drug release from a transdermal patch; for example, drug-loaded hydrogels can respond to the temperature change induced by light irradiation (**Figure 1.5d**).[72] Along with the increase in cumulative delivery, drug transport can be easily switched on and off by controlling the external stimuli.

Alternatively, mechanical force can control the release of drugs from the transdermal patch. The patch is fabricated with a drug-laden elastomer, and therefore, can be conformally attached to the finger joints.[73] The patch experiences lateral strain upon joint flexing, which subsequently releases the drug from the patch (**Figure 1.5e**).

External devices, particularly the wearable forms, can be integrated with drug-laden patches. The devices deliver sufficient energy to promote drug diffusion through the skin. Devices that operate with heat and electricity are frequently used as drug-delivering locomotives. For example, local heat from a wearable heater (**Figure 1.5f**) can enhance the skin permeation of drugs.[74] When the heat is applied, solubility and diffusivity of inorganic and organic drugs increase from the drug-containing layer (**Figure 1.5g**).[75] The application of heat also increases the circulation of body fluid, the permeability of blood vessel walls, and the rate-limiting membrane permeability, which in turn increases the permeation of the transdermally administered drugs. For example, the effect of temperature was evaluated *in vitro* by estimating the transdermal fentanyl (a potent opioid analgesic) flux at temperatures of 32 and 37°C. The drug flux approximately doubled over this 5°C increase in temperature. Further studies indicate that temperature

changes of approximately 5°C are necessary to cause a measurable change in cell membrane permeability and enhanced drug transport.

Iontophoresis uses an electrical current to enhance and control the penetration of charged drugs into tissues through the skin barrier (**Figure 1.5h**).[24] The dose is easily controlled by changing the magnitude of the stimulating current and the duration of charge induction. Application examples of the iontophoresis include administration of drugs for pain relief, for diagnosis of inflammation, chronic edema, and cystic fibrosis, and for cosmetic purposes. A weak electrical current below 500 μA cm^{-2} is applied to a skin area of a few centimeter squares to prevent pain, irritation, and skin burns. The electrical field increases the rate of drug transport compared to that of passive diffusion-based methods.[76] Recently, a cryoelectrophoresis technique was shown to increase the efficacy of electrophoresis by applying a strong current to locally frozen skin to eliminate the risk of skin burns.[77]

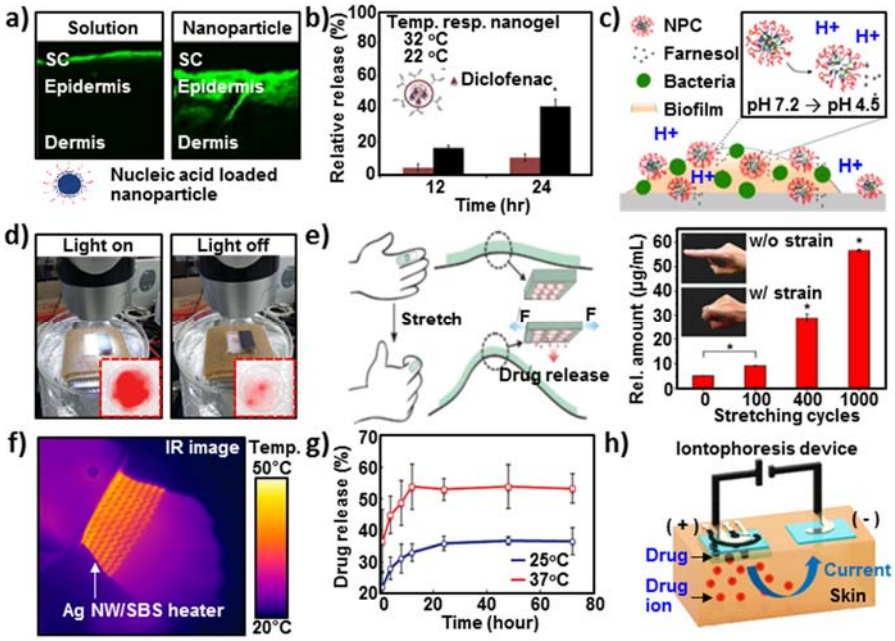

Figure 1.5. Second generation transdermal drug delivery. (a) Confocal images of solution-based (left) and nanoparticle (NP)-based (right) nucleic acid delivery via transdermal route. (b) Temperature responsive drug release from nanogel. (c) Schematic illustration of pH-responsive drug release. (d) Optical images of light responsive release. (e) Schematic illustration of stretch-triggered drug release (left). Accumulative drug release during 1000 cycles of finger flexion (right). (f) Infrared camera image of a wearable heater on the wrist. (g) Cumulative release of drugs from PNIPAM microparticles embedded on heater before (25 ^{o}C) and after (37 ^{o}C) thermal stimulation. (h) Schematic

illustration of iontophoresis treatment. (a) from Ref. [68], (b) from Ref. [70], (c) from Ref. [71], (d) from Ref. [72], (e) from Ref. [73], (f) from Ref. [74], (g) from Ref. [75], and (h) from Ref. [24].

1.3.3 Third-generation transdermal drug delivery technology

Extensive efforts have been invested in developing strategies to deliver drugs through the skin without damaging the stratum corneum such as the incorporation of chemical enhancers, application of heat, and iontophoretic methods. However, an alternative approach that involves destroying the stratum corneum is rapidly being adopted because disrupting the epidermis to a clinically safe level would enable the delivery of a large number of hydrophilic drugs and macromolecules across the skin.[78] High power energy modalities (*e.g.*, radiofrequency (RF), ultrasound, and laser techniques) and various types of microneedles are currently used to disrupt or puncture the skin and enhance drug delivery. However, destruction of the skin should be minimized and carefully controlled to allow its rapid recovery.[79]

Disruption of the epidermis by high power energy broadens the range of drugs that can be delivered through the skin.[78] Because a significantly high level of energy is required to damage the outer layers of skin, it is necessary to carefully control the amplitude and exposure time of the applied energy to prevent unwanted damage to the inner skin layers. RF ablation uses a high-frequency electrical current (100-500 kHz) for localized heating of the outer skin layer (**Figure 1.6a**).[80] Sonophoresis

uses ultrasound which generates heat and promotes drug delivery into the skin.[47,81,82] Recently, double frequency ultrasound was used to enhance the skin permeability and shorten the treatment time compared to single frequency ultrasound (**Figure 1.6b**).[83] Laser ablation is also commonly used in cosmetics for procedures such as hair removal, skin resurfacing, and acne treatment. The laser targets a high level of energy at a designated location to penetrate the skin.[84,85] Gold nanorods absorb near-infrared light and generate an intense heat, which can damage the outer layer of the skin. The pulsed laser only increases the temperature of the skin surface and causes less damage to the inner skin than continuous-wave laser does (**Figure 1.6c**).[86-88]

Although RF ablation, sonophoresis, and laser ablation methods show reasonably high potentials, they need bulky and expensive equipment and thus can only be performed at clinics. As an alternative, microneedles have attracted considerable attention because they can transport drugs in a minimally invasive manner via the transdermal route, and are relatively simple and cheap.[79,89] Microneedles are easier to use and less painful to the skin than high-power energy modalities. In addition, microneedles enable the controlled and sustained release of drugs depending on the patients' needs. Microneedles are divided into

several types according to their shape and use including solid, surface-coated, dissolvable, hollow-shaped, and smart microneedles. Solid microneedles are fabricated from hard materials such as silicon and metals.[90-93] The hardness of the materials enables the solid microneedles to easily create micropores, which are the micro-inlet through which drugs are transferred. The micropores are recovered a short period after the creation and, therefore, additional patches or drugs (*e.g.*, diclofenac) can be used to extend the duration of the formed micropores.

Microneedles may also incorporate a drug coated onto the surface of the solid needle substrate (**Figure 1.6d**).[94,95] Since the coating layer decreases the physical strength and sharpness of needles, the drug load on the needle surface is limited to a small amount. Accordingly, coated microneedles are used for treatments where large amounts of drugs are not required to be delivered (*e.g.,* vaccine delivery and cosmetic procedures).[96,97]

Dissolvable microneedles are formulated from water-soluble and biocompatible polymers. In dissolvable microneedles, drugs are embedded in the polymeric matrix and released as the matrix degrades or dissolves slowly in body fluids (**Figure 1.6e**).[98-103] The temporal drug

release profile can be controlled from several seconds to several months by selecting appropriate polymers. However, there are also challenges associated with this technique. For example, the use of ultraviolet (UV) irradiation or elevated temperature to cure the polymer for microneedles during the fabrication process can denature the drugs loaded in the polymeric precursor. The drug quantity that can be loaded into the polymeric matrix is also limited because a high percentage of drug in the precursor mixture would undermine the mechanical strength of the needles.

Hollow microneedles have a hollow core inside the needle through which the drug solution flows (**Figure 1.6f**).[104-107] The drug solution can be delivered passively by diffusion or actively by pressure-driven flow through the needle hole. A drug reservoir attached to the back of the microneedles releases the drug by the action of a pump. Hollow microneedles have a merit in controlling the amount of injected drug. However, one disadvantage of this approach is that additional equipment (*e.g.*, drug reservoir and pump) assisting the microneedles are required for drug delivery.[78]

Smart microneedle systems, which are sensitive to external and internal stimuli, have also been studied for use as controlled transdermal drug

delivery systems. Smart microneedles can provide patient-friendly and feedback-controlled drug delivery, which has not been accomplished with previous microneedle systems. Microneedles that are responsive to external stimuli (*e.g.*, heat, laser, and mechanical strain) provide an on/off trigger for drug administration, which can be easily controlled by patients.[50,73] An example is the mechanically responsive microneedles whose drug release is modulated by lateral strain (**Figure 1.6g**).[73] The microneedles that release the drug payload following lateral pulling were successfully tested *in vivo*. Smart NPs that are responsive to biochemical stimuli (*e.g.*, pH change, glucose concentration, and hypoxia) can also be loaded in microneedles (**Figure 1.6h left**).[52,108,109] Microneedles facilitate the entry of NPs into the bloodstream, and the delivered NPs respond to the patient's physiological state and release the drugs accordingly. The concept has been demonstrated by NPs containing glucose oxidase, which release insulin in response to a high blood glucose concentration to modulate its level (**Figure 1.6h right**).[108]

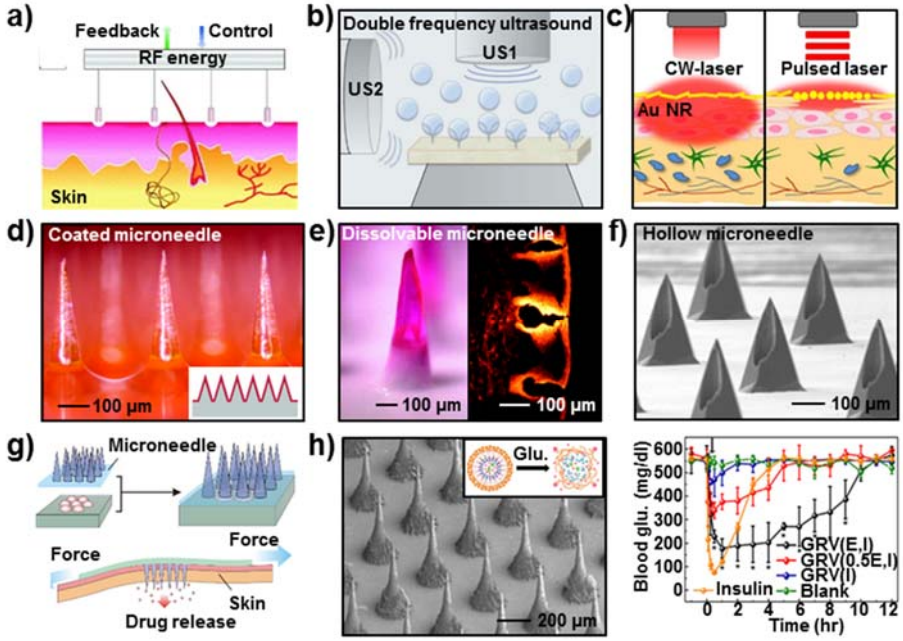

Figure 1.6. Third generation transdermal drug delivery (a) Schematic illustration of radiofrequency (RF) ablation on skin. (b) Schematic illustration of double frequency ultrasonic treatment for transdermal drug delivery. (c) Schematic illustration of gold nanorod (AuNR) assisted photothermal ablation with continuous-wave (CW) (left) and pulsed laser (right). (d) Optical microscopic image of sucrose-coated polylactic acid microneedles. Schematic illustration of coated microneedles (inset). (e) Optical image of dissolvable microneedles (left). Fluorescence microscopic image of porcine skin after poration of microneedles (right). (f) SEM image of hollow microneedles. (g)

Schematic illustrations of strain-responsive microneedles. (h) SEM images of smart NP-loaded microneedles (left). Schematic illustration of glucose-responsive drug release (inset). Blood glucose level changes after microneedle patch treatment (right). (a) from Ref. [80], (b) from Ref. [83], (c) from Ref. [86], (d) from Ref. [95], (e) from Ref. [99], (f) from Ref. [104], (g) from Ref. [73], and (h) from Ref. [108].

1.4 Fourth-generation transdermal drug delivery technology

To date, previous research on transdermal drug delivery has focused on enhancing the amount of drug transported across the skin barrier. However, in recent years, the research focus has shifted to the controlled and patterned release of drug doses in response to patients' health conditions. In line with this perspective, fourth generation transdermal drug delivery strategies feature real-time monitoring of the biometric information using a wearable device system. Wearable biosensors promote customized therapy for each patient since the sensors determine when the drug is released, how much of the dose is required, and whether the physiological feedback calls for additional drug release.

1.4.1 Transdermal drug delivery based on physiological/electrophysiological monitoring

To diagnose the health condition of an individual, an assortment of physical and electrical cues must be collected first. The collection of precise health information with high spatiotemporal resolution is

important in controlling drug delivery. Since the surface of the skin is soft, curvilinear, and movable, skin-mounted sensors necessitate physical characteristics similar to those of the skin to obtain high-quality information without motion artifacts or background noises from the skin surface. Flexible and stretchable devices in ultrathin and serpentine structures facilitate a conformal contact with the skin, which is crucial for high fidelity measurement of bodily signals.[28,54,55] Therefore, attached soft wearable biosensors that conform to skin contours enable the precise real-time monitoring of an individual's physiological biomarker without hindering bodily motions. Accurate diagnosis based on the conformal skin contact also contributes to the controlled transdermal release of drugs actuated by the monitoring devices as a physiological feedback.

Physiological signals such as body temperature,[6] motion information including tremors,[3,9,10] and heart movements[5,7,8,19] are the key information required for diagnosing the health condition of an individual. Collected signals can be used for patient-customized transdermal drug delivery. For example, a multifunctional and wearable patch monitors movement disorders continuously using silicon membrane-based strain gauges, and stores the recorded information on the activities and tremors

in the memory module.[3] Continuously operating sensors collect vital signals and the cumulative information is processed to operate a co-integrated drug delivery unit (**Figure 1.7a**). According to the patient's health condition, wearable drug actuators trigger drug delivery through the skin. To maximize the amount of loaded drugs, mesoporous silica NPs (MSNs) serve as the drug delivery vehicles in the patch because their large surface area allows greater drug adsorption. The programmable thermal actuators control the drug delivery through the skin by enhancing drug diffusion (**Figure 1.7b**). The generated heat degrades the binding of the MSNs and the loaded drugs, which subsequently diffuse transdermally (**Figure 1.7c**). The integrated temperature sensor conducts real-time monitoring to prevent any low-temperature burns.

Electrical signals are also an integral part of health monitoring that enables relevant information to be collected continuously. The time-dependent amplitude and wave pattern of electrophysiological signals such as those of an electromyogram, electroencephalogram, and electrocardiogram indicate the condition of the muscles, brain, and heart, respectively in real-time. These signals can be detected from the outer skin noninvasively using wearable electrodes and a co-integrated

amplifier.[19] To investigate the reliable long-term monitoring of signals, some studies have focused on the interface between wearable device and tissues to establish a robust mechanical coupling for a highly sensitive and accurate biometric detection.[5,8] The design motifs based on bio-inspired interfaces enable sufficient adhesion to the skin without using adhesive glues that may cause skin irritation with long-term use. Based on the measured electrical signals, the integrated drug actuators can efficiently deliver the loaded drug through the skin (**Figure 1.7d**).[5] For electrostatically charged drugs, iontophoresis can serve as an efficient delivery method. In a study, MSNs were also used as drug delivery vehicles to prevent oxidation, denaturation, and unstimulated diffusion of drugs. Iontophoretic delivery accelerates the deep permeation of the drug into the skin, mediated by the charge repulsion between the electrodes and drugs (**Figure 1.7e**). Iontophoretic actuation of drug-loaded MSNs enhanced the skin penetration significantly compared to those of the control and thermal diffusion (**Figure 1.7f**). Iontophoresis also has advantages over thermal diffusion by preventing low-temperature burns on the skin and thermal denaturation of the loaded drugs.

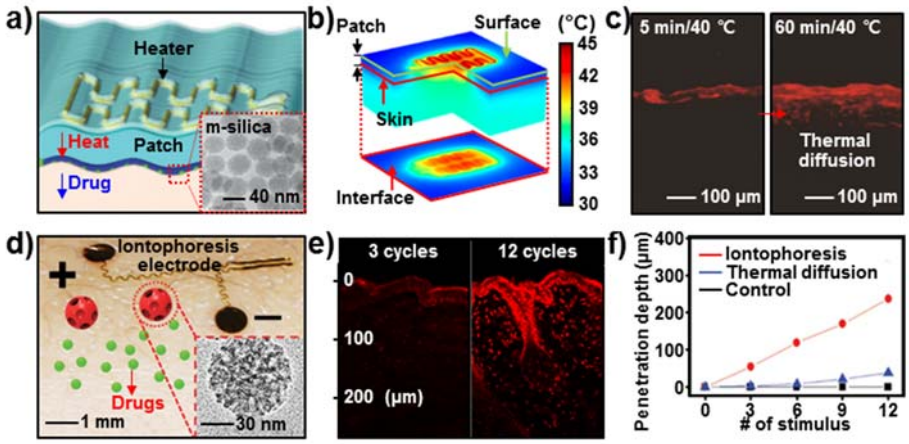

Figure 1.7. Enhanced transdermal drug delivery. (a) Transdermal drug delivery using a wearable heater. Drug loaded in mesoporous silica NPs (MSNs) is released by thermal stimulation. (b) Finite element modelling of the three-dimensional thermal profile of a heater on the patch and at the interface between the patch and the human skin. (c) Cross-sectional fluorescence images shows enhanced drug diffusion into pig skin via thermal actuation. (d) Transdermal drug delivery using the iontophoresis. (e) Cross-sectional fluorescence images for the drug (doxorubicin) diffusion into the mouse skin with different stimuli of iontophoresis; 3 cycles (left) and 12 cycles (right). (f) Stimulus number versus drug diffusion length into the mouse skin with different actuators (black: none,

blue: thermal actuator, and red: iontophoresis electrode). (a-c) from Ref. [3], and (d-f) from Ref. [5].

1.4.2 Transdermal drug delivery based on biochemical signal monitoring

Biochemical analysis of biofluids can provide ample information on an individual's health condition and disease progression.[22-27] For wearable devices, sweat is frequently used as a specimen to monitor the physiological and biochemical conditions such as glucose level because it contains voluminous metabolic data (**Figure 1.8a**).[110-113] In accordance with the versatility of sweat analysis in disease diagnosis, wearable sweat sensors are developed to conveniently measure the analytes of interest.

Wearable and disposable chemical sensors are recently developed examples based on colorimetric and electrochemical analyses. Colorimetric analysis is widely used for simple and disposable sensing instruments because the presence of biomarkers is easily confirmed by color changes (**Figure 1.8b**).[114,115] Although this method can be used to monitor various biomarkers such as perspiration rate, total sweat loss, pH, chlorides, and lactates, it is difficult to accurately quantify the color changes to determine the exact concentration of the biomarkers. Wearable electrochemical sensors have been devised to quantifiably detect biomarkers in the sweat. The concentration of target biomarkers

is directly measured based on the electrical signals from the redox reaction of the markers in a short time. The wearable electrochemical sensors fabricated using screen printing have simple structures and enable the facile measurement of single biomarkers (**Figure 1.8c**).[111] An array of electrochemical sensors is also available for the simultaneous detection of multiple biomarkers.[26] The information acquired from the sweat is wirelessly collected and continuously stored in mobile devices for long-term health monitoring.

Accurate monitoring of the sweat glucose level is of primary interest because of its direct correlation to the blood glucose level.[116] Furthermore, this correlation inspired the development of a skin-based diabetes control system that combines sweat glucose detection with microneedle-based drug delivery for minimally invasive blood glucose regulation.[112,113] Conventional blood glucose monitoring for diabetes inflicts pain and stress during the blood withdrawal and drug injection steps. Therefore, device-assisted glucose monitoring and feedback therapy could improve the quality of life of patients with diabetes by managing blood glucose level more conveniently. The minimally invasive glucose monitoring system is initiated by perspiration after the patch is applied (**Figure 1.8d left**). To measure the sweat glucose level

more accurately, data collected from the glucose sensor are corrected by integrated pH, temperature, and humidity sensors. It ensures that corrections are made for the activity variation of glucose oxidase, which is the primary detection moiety (**Figure 1.8d middle**). When hyperglycemia occurs, the microneedles are triggered by the sensor signal to transdermally administer the antidiabetic drug (**Figure 1.8d right**).

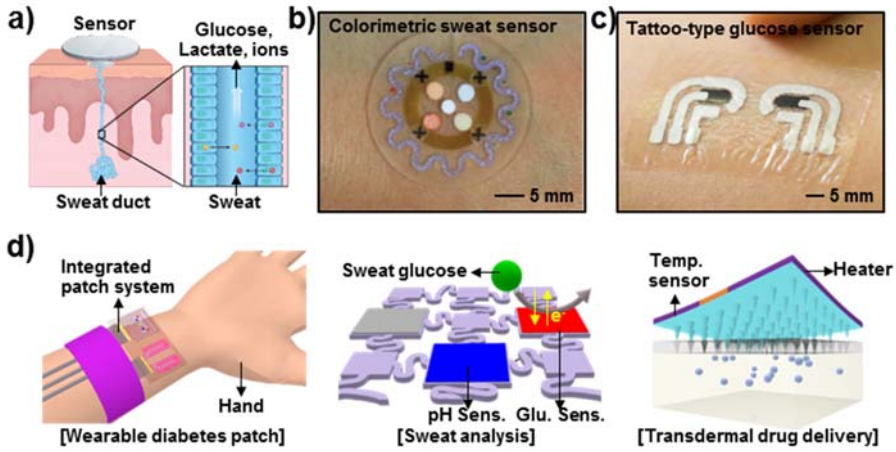

Figure 1.8. Biochemical signal monitoring. (a) Schematic illustration of sweat monitoring system on the skin. Biomarkers such as glucose, lactate, and ions secrete from epithelial cells along the sweat ducts inside the skin, reflecting a subject's physiological state. (b) Optical image of colorimetric sweat sensor mounted on the forearm. (c) Optical image of a sweat glucose monitoring tattoo device applied to a human subject. (d) Schematic illustrations of operation process of skin-based diabetes monitoring and therapy system. (a) from Ref. [100], (b) from Ref. [114], (c) from Ref. [26], and (d) from Ref. [112].

1.4.3 Temperature-responsive Transdermal Drug Delivery

In the case of conventional microneedles, it was difficult to control the duration and amount of the drug dose released because the drug diffusion is irreversible once the microneedles are inserted into the skin. In addition, data to determine the drug delivery rate are unavailable. Recent studies have demonstrated the prospect of controlled transdermal drug release based on real-time health monitoring using a wearable device-assisted thermo-responsive microneedles system.[112,113] Phase change materials (PCMs) protect the drug and dissolvable microneedle matrix from biofluids below the critical melting temperature (**Figure 1.9b**). When multi-channel heaters initiate patterned thermal actuation, the PCM coating on the microneedles melts, and thereby, the transdermal drug delivery proceeds by partial or total dissolution of the microneedles (**Figure 1.9c**). The amount of delivered drug can be controlled by the area of the applied heating, which is determined by the integrated wearable biosensors. Temperature sensors near the heater simultaneously monitor the temperature variation of the heaters to sequentially control the drug release and prevent low-temperature burns.

For precisely-controlled drug delivery system, the phase change nanoparticle(PCN)s are synthesized. Different PCNs can vary critical

temperature of actuations, which enables multi-stage drug delivery with actuation of heaters. By using PCNs combined with drugs and multichannel heaters, the drug delivery system features a controlled transdermal release of drugs at up to six different release amounts. The effectiveness of the wearable microneedle system was demonstrated in diabetic (db/db) mice by triggering controlled transcutaneous drug release using thermal actuators. Animal experiments with diabetic mice confirmed the efficacy of the microneedles in reducing blood glucose levels. The next-generation transdermal drug delivery systems are a considerable improvement on wearable devices that have a limited ability to detect or treat disease conditions. Furthermore, the next-generation transdermal drug delivery represents the integration of multiple functionalities in a single device. In addition, the interactive and complementary co-application of sensing and therapy to enable patient-customized transdermal drug delivery will likely be available in the foreseeable future through the next-generation systems.

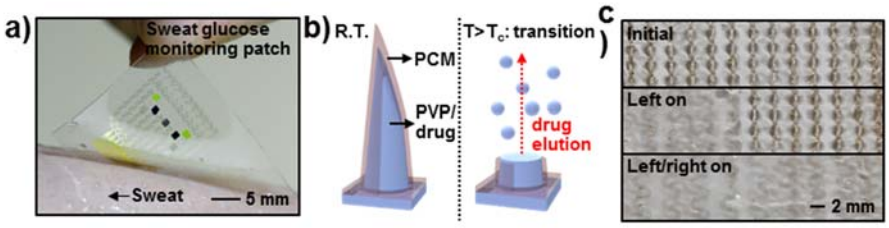

Figure 1.9. Temperature-responsive transdermal drug delivery. (a) Optical image of multifunctional electrochemical devices on the human skin with perspiration. (b) Schematic illustrations of drug-loaded bioresorbable microneedles. The phase change material (PCM) coating prevents unwanted drug release before programmed thermal actuation. (c) Optical images of the stepwise dissolution of the microneedles for drug dose control. (a-c) from Ref. [112].

1.5 Conclusion

The skin, which has long been perceived as unsuitable for drug delivery, currently widens the vista on the possibilities for drug delivery strategies with its physiological significance and convenience. Studies to overcome the challenges of the skin barrier against drug permeation and improve the efficiency of transdermal drug delivery have shown considerable success as demonstrated by the first, second, and third generations of transdermal delivery strategies. From simple patches to intricate microneedles, diverse approaches to improve the efficiency of drug delivery are still in progress. Amidst the rising popularity of the transdermal route, the device-assisted transdermal delivery system provides a new paradigm for drug delivery in response to the real-time progression of disease.

The diagnosis of the health status of patients using wearable sensors and the drug administration that is finely and timely controlled by actuators are combined with the detection of physiological changes by sensors to provide a complete feedback therapy. This strategy is expected to enhance the quality and effectiveness of medical therapy. Since the previous generations of the transdermal drug delivery technology have

focused on maximizing the efficiency of delivery, this novel technological platform complements the drawbacks of previous transdermal delivery systems and even yields synergetic results when the most advanced transdermal patches and devices are combined altogether.

Furthermore, integration of flexible heaters or devices with thermo-responsive drug delivery system can provide precise and controlled transdermal drug delivery. Temperature-responsive nanoparticles or microneedles can block the unwanted drug release before actuation of heaters, which is important for maintenance of homeostasis. Also, heaters can accelerate the drug transportation through skin.

Since the incorporation of wearable sensors and advanced transdermal patch formulations is still in the early stage, there is a spacious room for future research aimed at improving the wearable devices and rigorously optimizing the reliability of the system, as well as their application to assorted disease models. Continued efforts to enhance the delivery of drugs that are considered unsuitable for administration through the skin (*e.g.*, peptides, nucleic acids, and macromolecules) must also be carried out to broaden the library of transdermally applicable drugs. Although the patient-customized transdermal drug delivery still requires much development, this approach holds great promise for the convenient

management of diseases in daily life and a novel paradigm for healthcare in the future.

Most of the contents of this chapter were published in the article, "Device-assisted Transdermal Drug Delivery." (*Advanced Drug Delivery Reviews* **2017, *submitted*)

1.6 References

[1] Prausnitz, M. R.; Langer, R. *Nat. Biotechnol.*, **2008**, *26*, 1261.

[2] Oosten, A. W.; Abrantes, J. A.; Jonsson, S.; de Bruijn, P.; Kuip, E. J.; Falcao, A.; van der Rijt, C. C.; Mathijssen, R. H. Eur. *J. Clin. Pharmacol.*, **2016**, *72*, 459.

[3] Son, D.; Lee, J.; Qiao, S.; Ghaffari, R.; Kim, J.; Lee, J. E.; Song, C.; Kim, S. J.; Lee, D. J.; Jun, S. W.; Yang, S.; Park, M.; Shin, J.; Do, K.; Lee, M.; Kang, K.; Hwang, C. S.; Lu, N.; Hyeon, T.; Kim, D.-H. *Nat. Nanotech.*, **2014**, *9*, 397.

[4] Choi, M. K.; Park, I.; Kim, D. C.; Joh, E.; Park, O. K.; Kim, J.; Kim, M.; Choi, C.; Yang, J.; Cho, K. W.; Hwang, J.-H.; Nam, J.-M.; Hyeon, T.; Kim, J. H.; Kim, D.-H. *Adv. Funct. Mater.*, **2015**, *25*, 7109.

[5] Choi, M. K.; Park, O. K.; Choi, C.; Qiao, S.; Ghaffari, R.; Kim, J.; Lee, D. J.; Kim, M.; Hyun, W.; Kim, S. J.; Hwang, H. J.; Kwon, S. H.; Hyeon, T.; Lu, N.; Kim, D.-H. *Adv. Healthc. Mater.*, **2016**, *5*, 80.

[6] Webb, R. C.; Bonifas, A. P.; Behnaz, A.; Zhang, Y.; Yu, K. J.; Cheng, H.; Shi, M.; Bian, Z.; Liu, Z.; Kim, Y. S.; Yeo, W. H.; Park, J. S.; Song, J.; Li, Y.; Huang, Y.; Gorbach, A. M.; Rogers, J. A. *Nat. Mater.*, **2013**, *12*, 938.

[7] Schwartz, G.; Tee, B. C.; Mei, J.; Appleton, A. L.; Kim, D. H.; Wang, H.;

Bao, Z. *Nat. Commun.*, **2013**, *4*, 1859.

[8] Pang, C.; Koo, J. H.; Nguyen, A.; Caves, J. M.; Kim, M. G.; Chortos, A.; Kim, K.; Wang, P. J.; Tok, J. B.; Bao, Z. *Adv. Mater.*, **2015**, *27*, 634.

[9] Kim, J.; Lee, M.; Shim, H. J.; Ghaffari, R.; Cho, H. R.; Son, D.; Jung, Y. H.; Soh, M.; Choi, C.; Jung, S.; Chu, K.; Jeon, D.; Lee, S. T.; Kim, J. H.; Choi, S. H.; Hyeon, T.; Kim, D.-H. *Nat. Commun.*, **2014**, *5*, 5747.

[10] Lim, S.; Son, D.; Kim, J.; Lee, Y. B.; Song, J.-K.; Choi, S.; Lee, D. J.; Kim, J. H.; Lee, M.; Hyeon, T.; Kim, D.-H. *Adv. Funct. Mater.,* **2015**, *25*, 375.

[11] Jung, S.; Kim, J. H.; Kim, J.; Choi, S.; Lee, J.; Park, I.; Hyeon, T.; Kim, D.-H. *Adv. Mater.*, **2014**, *26*, 4825.

[12] Jung, S.; Lee, J.; Hyeon, T.; Lee, M.; Kim, D.-H. *Adv. Mater.*, **2014**, *26*, 6329.

[13] Yang, H.; Qi, D.; Liu, Z.; Chandran, B. K.; Wang, T.; Yu, J.; Chen, X. *Adv. Mater.*, **2016**, *28*, 9175.

[14] Wang, T.; Guo, Y.; Wan, P.; Sun, X.; Zhang, H.; Yu, Z.; Chen, X. *Nanoscale*, **2017**, *9*, 869.

[15] Kaltenbrunner, M.; Sekitani, T.; Reeder, J.; Yokota, T.; Kuribara, K.; Tokuhara, T.; Drack, M.; Schwodiauer, R.; Graz, I.; Bauer-Gogonea, S.; Bauer, S.; Someya, T. *Nature*, **2013**, *499*, 458.

[16] Kim, D.-H.; Lu, N.; Ma, R.; Kim, Y.-S.; Kim, R.-H.; Wang, S.; Wu, J.;

Won, S. M.; Tao, H.; Islam, A.; Yu, K. J.; Kim, T.-I.; Chowdhury, R.; Ying, M.; Xu, L.; Li, M.; Chung, H.-J.; Keum, H.; McCormick, M.; Liu, P.; Zhang, Y.-W.; Omenetto, F. G.; Huang, Y.; Coleman, T.; Rogers, J. A. *Science*, **2011**, *333*, 838.

[17] Xu, S.; Zhang, Y.; Jia, L.; Mathewson, K. E.; Jang, K.-I.; Kim, J.; Fu, H.; Huang, X.; Chava, P.; Wang, R. *Science*, **2014**, *344*, 70.

[18] Jang, K.-I.; Chung, H. U.; Xu, S.; Lee, C. H.; Luan, H.; Jeong, J.; Cheng, H.; Kim, G.-T.; Han, S. Y.; Lee, J. W. *Nat. commun.*, **2015**, *6*.

[19] Kim, J.; Son, D.; Lee, M.; Song, C.; Song, J.-K.; Koo, J. H.; Lee, D. J.; Shim, H. J.; Kim, J. H.; Lee, M. *Sci. Adv.*, **2016**, *2*, e1501101.

[20] Sekitani, T.; Yokota, T.; Kuribara, K.; Kaltenbrunner, M.; Fukushima, T.; Inoue, Y.; Sekino, M.; Isoyama, T.; Abe, Y.; Onodera, H. *Nat. commun.*, **2016**, *7*.

[21] Park, J.; Choi, S.; Janardhan, A. H.; Lee, S.-Y.; Raut, S.; Soares, J.; Shin, K.; Yang, S.; Lee, C.; Kang, K.-W.; Cho, H. R.; Kim, S. J.; Seo, P.; Hyun, W.; Jung, S.; Lee, H.-J.; Lee, N.; Choi, S. H.; Sacks, M.; Lu, N.; Josephson, M. E.; Hyeon, T.; Kim, D.-H.; Hwang, H. J. *Sci. Transl. Med.*, **2016**, *8*, 344ra386.

[22] Bandodkar, A. J.; Hung, V. W.; Jia, W.; Valdes-Ramirez, G.; Windmiller, J. R.; Martinez, A. G.; Ramirez, J.; Chan, G.; Kerman, K.; Wang, J. *Analyst*,

2013, *138*, 123.

[23] Jia, W.; Bandodkar, A. J.; Valdes-Ramirez, G.; Windmiller, J. R.; Yang, Z.; Ramirez, J.; Chan, G.; Wang, J. *Anal. Chem.*, **2013**, *85*, 6553.

[24] Kim, J.; Jeerapan, I.; Imani, S.; Cho, T. N.; Bandodkar, A.; Cinti, S.; Mercier, P. P.; Wang, J. *ACS Sens.*, **2016**, *1*, 1011.

[25] Rose, D. P.; Ratterman, M. E.; Griffin, D. K.; Hou, L.; Kelley-Loughnane, N.; Naik, R. R.; Hagen, J. A.; Papautsky, I.; Heikenfeld, J. C. *IEEE Transactions on Biomedical Engineering*, **2015**, *62*, 1457.

[26] Gao, W.; Emaminejad, S.; Nyein, H. Y.; Challa, S.; Chen, K.; Peck, A.; Fahad, H. M.; Ota, H.; Shiraki, H.; Kiriya, D.; Lien, D. H.; Brooks, G. A.; Davis, R. W.; Javey, A. *Nature*, **2016**, *529*, 509.

[27] Gao, W.; Nyein, H. Y. Y.; Shahpar, Z.; Fahad, H. M.; Chen, K.; Emaminejad, S.; Gao, Y.; Tai, L.-C.; Ota, H.; Wu, E.; Bullock, J.; Zeng, Y.; Lien, D.-H.; Javey, A. *ACS Sens.*, **2016**, *1*, 866.

[28] Choi, S.; Lee, H.; Ghaffari, R.; Hyeon, T.; Kim, D.-H. *Adv. Mater.*, **2016**, *28*, 4203.

[29] Choi, M. K.; Yang, J.; Kang, K.; Kim, D.C.; Choi, C.; Park, C.; Kim, S. J.; Chae, S. I.; Kim, T. H.; Kim, J. H.; Hyeon, T.; Kim, D.-H. *Nat. Commun.*, **2015**, *6*, 7149.

[30] Son, D.; Koo, J. H.; Song, J.-K.; Kim, J.; Lee, M.; Shim, H. J.; Park, M.;

Lee, M.; Kim, J. H.; Kim, D.-H. *ACS nano*, **2015**, *9*, 5585.

[31] Yokota, T.; Zalar, P.; Kaltenbrunner, M.; Jinno, H.; Matsuhisa, N.; Kitanosako, H.; Tachibana, Y.; Yukita, W.; Koizumi, M.; Someya, T. *Sci. Adv.*, **2016**, *2*, e1501856.

[32] Wang, H.; Pastorin, G.; Lee, C. *Adv. Sci.*, **2016**, *3*, 1500441.

[33] Tao, H.; Hwang, S. W.; Marelli, B.; An, B.; Moreau, J. E.; Yang, M.; Brenckle, M. A.; Kim, S.; Kaplan, D. L.; Rogers, J. A.; Omenetto, F. G. *Proc. Natl. Acad. Sci. USA*, **2014**, *111*, 17385.

[34] Rein, H. *Z. Biol.*, **1924**, *81*, 125.

[35] Scheuplein, R. J.; Blank, I. H. *Physiol. Rev.*, **1971**, *51*, 702.

[36] Cramer, M. P.; Saks, S. R. *Pharmacoeconomics*, **1994**, *5*, 482.

[37] Lane, M. E. *Int. J. Pharm.*, **2013**, *447*, 12.

[38] Alexander, A.; Dwivedi, S.; Ajazuddin,; Giri, T.K.; Saraf, S.; Saraf, S.; Tripathi, D. K. *J. Control. Release*, **2012**, *164*, 26.

[39] Prow, T. W.; Grice, J. E.; Lin, L. L.; Faye, R.; Butler, M.; Becker, W.; Wurm, E. M.; Yoong, C.; Robertson, T. A.; Soyer, H. P.; Roberts, M. S. *Adv. Drug. Deliv. Rev.*, **2011**, *63*, 470.

[40] Ge, S.; Lin, Y.; Lu, H.; Li, Q.; He, J.; Chen, B.; Wu, C.; Xu, Y. *Int. J. Pharm.*, **2014**, *465*, 120.

[41] Lai, F.; Pireddu, R.; Corrias, F.; Fadda, A. M.; Valenti, D.; Pini, E.; Sinico,

C. *Int. J. Pharm.*, **2013**, *458*, 104.

[42] Elnaggar, Y. S.; El-Refaie, W. M.; El-Massik, M. A.; Abdallah, O. Y. *J. Control. Release*, **2014**, *180*, 10.

[43] Teodorescu, F.; Queniat, G.; Foulon, C.; Lecoeur, M.; Barras, A.; Boulahneche, S.; Medjram, M. S.; Hubert, T.; Abderrahmani, A.; Boukherroub, R.; Szunerits, S. *J. Control. Release*, **2017**, *245*, 137.

[44] Cazares-Delgadillo, J.; Ganem-Rondero, A.; Merino, V.; Kalia, Y. N. *Eur. J. Pharm. Sci.*, **2016**, *85*, 31.

[45] Pereira, T. A.; Ramos, D. N.; Lopez, R. F. *Sci. Rep.*, **2017**, *7*, 44236.

[46] Kim, J.; Jang, J. H.; Lee, J. H.; Choi, J. K.; Park, W. R.; Bae, I. H.; Bae, J.; Park, J. W. *Pharm. Res.*, **2012**, *29*, 2017.

[47] Schoellhammer, C. M.; Srinivasan, S.; Barman, R.; Mo, S. H.; Polat, B. E.; Langer, R.; Blankschtein, D. *J. Control. Release*, **2015**, *202*, 93.

[48] Haedersdal, M.; Erlendsson, A. M.; Paasch, U.; Anderson, R. R. *J. Am. Acad. Dermatol.*, **2016**, *74*, 981.

[49] Lee, W. R.; Shen, S. C.; Aljuffali, I. A.; Li, Y.C.; Fang, J.Y. *Pharm. Res.*, **2014**, *31*, 382.

[50] Chen, M. C.; Lin, Z. W.; Ling, M. H. *ACS nano*, **2016**, *10*, 93.

[51] Hirobe, S.; Azukizawa, H.; Hanafusa, T.; Matsuo, K.; Quan, Y. S.; Kamiyama, F.; Katayama, I.; Okada, N.; Nakagawa, S. *Biomaterials*, **2015**,

57, 50.

[52] Wang, C.; Ye, Y.; Hochu, G. M.; Sadeghifar, H.; Gu, Z. *Nano. Lett.*, **2016**, *16*, 2334.

[53] Edens, C.; Dybdahl-Sissoko, N. C.; Weldon, W. C.; Oberste, M. S.; Prausnitz, M. R. *Vaccine*, **2015**, *33*, 4683.

[54] Someya, T.; Bao, Z.; Malliaras, G. G. *Nature*, **2016**, *540*, 379.

[55] Kim, J.; Ghaffari, R.; Kim, D.-H. *Nat. Biomed. Eng.*, **2017**, *1*, 0049.

[56] Yang, J.; Choi, M.K.; Kim, D.-H.; Hyeon, T. *Adv. Mater.*, **2016**, *28*, 1176.

[57] D.W. Sifton, *Medical Economics/Thomson Healthcare* **2002**.

[58] Prausnitz, M. R.; Mitragotri, S.; Langer, R. *Nat. Rev. Drug. Discov.*, **2004**, *3*, 115.

[59] Mathur, V.; Satrawala, Y.; Rajput, M. *Asian J. Pharm.*, **2010**, *4*, 173.

[60] Batheja, P.; Sheihet, L.; Kohn, J.; Singer, A. J.; Michniak-Kohn, B. *J. Control. Release.,* **2011**, *149*, 159.

[61] Chen, H.; Chang, X.; Weng, T.; Zhao, X.; Gao, Z.; Yang, Y.; Xu, H.; Yang, X. *J. Control. Release*, **2004**, *98*, 427.

[62] Honeywell-Nguyen, P. L.; Bouwstra, J. A. V *Drug. Discov. Today Technol.*, **2005**, *2*, 67.

[63] Lee, H.; Lee, Y.; Song, C.; Cho, H. R.; Ghaffari, R.; Choi, T. K.; Kim, K. H.; Lee, Y. B.; Ling, D.; Lee, H.; Yu, S. J.; Choi, S. H.; Hyeon, T.; Kim,

D.-H. *Nat. Commun.*, **2015**, *6*, 10059.

[64] Shin, J.; Shin, K.; Lee, H.; Nam, J. B.; Jung, J. E.; Ryu, J. H.; Han, J. H.; Suh, K. D.; Kim, Y. J.; Shim, J.; Kim, J.; Han, S. H.; Char, K.; Kim, Y. K.; Chung, J. H.; Lee, M. J.; Kang, B. C.; Kim, J. W. *Adv. Mater.*, **2010**, *22*, 739.

[65] Marepally, S.; Boakye, C. H.; Patel, A. R.; Godugu, C.; Doddapaneni, R.; Desai, P. R.; Singh, M. *Nanomedicine*, **2014**, *9*, 2157.

[66] Zheng, D.; Giljohann, D. A.;. Chen, D. L.; Massich, M. D.; Wang, X.-Q.; Iordanov, H.; Mirkin, C.A.; Paller, A.S. *Proc. Natl. Acad. Sci. USA*, **2012**, *109*, 11975.

[67] Son, D.; Lee, J.; Lee, D. J.; Ghaffari, R.; Yun, S.; Kim, S. J.; Lee, J. E.; Cho, H. R.; Yoon, S.; Yang, S.; Lee, S.; Qiao, S.; Ling, D.; Shin, S.; Song, J.-K.; Kim, J.; Kim, T.; Lee, H.; Kim, J.; Soh, M.; Lee, N.; Hwang, C. S.; Nam, S.; Lu, N.; Hyeon, T.; Choi, S. H.; Kim, D.-H. *ACS Nano*, **2015**, *9*, 5937.

[68] Desai, P. R.; Marepally, S.; Patel, A. R.; Voshavar, C.; Chaudhuri, A.; Singh, M. *J. Control. Release*, **2013**, *170*, 51.

[69] Ling, D.; Xia, H.; Park, W.; Hackett, M. J.; Song, C.; Na, K.; Hui, K. M.; Hyeon, T. *ACS nano*, **2014**, *8*, 8027.

[70] Carmona-Moran, C. A.; Zavgorodnya, O.; Penman, A. D.; Kharlampieva,

E.; Bridges, Jr., S. L.; Hergenrother, R.W.; Singh, J. A.; Wick, T. M. *Int. J. Pharm.*, **2016**, *509*, 465.

[71] Horev, B.; Klein, M. I.; Hwang, G.; Li, Y.; Kim, D.; Koo, H.; Benoit, D. S. *ACS nano*, **2015**, *9*, 2390.

[72] Kim, H.; Lee, H.; Seong, K. Y.; Lee, E.; Yang, S. Y.; Yoon, J. *Adv. Healthc. Mater.*, **2015**, *4*, 2071.

[73] Di, J.; Yao, S.; Ye, Y.; Cui, Z.; Yu, J.; Ghosh, T. K.; Zhu, Y.; Gu, Z. *ACS nano*, **2015**, *9*, 9407.

[74] Choi, S.; Park, J.; Hyun, W.; Kim, J.; Kim, J.; Lee, Y. B.; Song, C.; Hwang, H. J.; Kim, J. H.; Hyeon, T.; Kim D.-H. *ACS nano*, **2015**, *9*, 6626.

[75] Bagherifard, S.; Tamayol, A.; Mostafalu, P.; Akbari, M.; Comotto, M.; Annabi, N.; Ghaderi, M.; Sonkusale, S.; Dokmeci, M. R.; Khademhosseini, A. *Adv. Healthc. Mater.*, **2016**, *5*, 175.

[76] Ogawa, Y.; Kato, K.; Miyake, T.; Nagamine, K.; Ofuji, T.; Yoshino, S.; Nishizawa, M. *Adv. Healthc. Mater.*, **2015**, *4*, 506.

[77] Aloisi, A.; Matera, M.; Potenza, R.; Santoro, G.; Tuve, C.; Messina, A. *AIP Conference Proceedings*, *AIP*, **2000**, 19.

[78] Gratieri, T.; Alberti, I.; Lapteva, M.; Kalia, Y. N. *Eur. J. Pharm. Sci.*, **2013**, *50*, 609.

[79] van der Maaden, K.; Jiskoot, W.; Bouwstra, J. *J. Control. Release*, **2012**,

161, 645.

[80] Sintov, A. C.; Krymberk, I.; Daniel, D.; Hannan, T.; Sohn, Z. e.; Levin, G. *J. Control. Release*, **2003**, *89*, 311.

[81] Polat, B. E.; Hart, D.; Langer, R.; Blankschtein, D. *J. Control. Release*, **2011**, *152*, 330.

[82] Mitragotri, S.; Blankschtein, D.; Langer, R. *Science*, **1995**, *269*, 850.

[83] Schoellhammer, C. M.; Polat, B. E.; Mendenhall, J.; Maa, R.; Jones, B.; Hart, D. P.; Langer, R.; Blankschtein, D. *J. Control. Release*, **2012**, *163*, 154.

[84] Lee, J. W.; Gadiraju, P.; Park, J. H.; Allen, M. G.; Prausnitz, M. R. *J. Control. Release*, **2011**, *154*, 58.

[85] Weiss, R.; Hessenberger, M.; Kitzmuller, S.; Bach, D.; Weinberger, E. E.; Krautgartner, W. D.; Hauser-Kronberger, C.; Malissen, B.; Boehler, C.; Kalia, Y. N.; Thalhamer, J.; Scheiblhofer, S. *J. Control. Release*, **2012**, *162*, 391.

[86] Tang, H.; Kobayashi, H.; Niidome, Y.; Mori, T.; Katayama, Y.; Niidome, T. *J. Control. Release*, **2013**, *171*, 178.

[87] Ramadan, S.; Guo, L.; Li, Y.; Yan, B.; Lu, W. *Small*, **2012**, *8*, 3143.

[88] Jung, H. S.; Kong, W. H.; Sung, D. K.; Lee, M.-Y.; Beack, S. E.; Keum, D. H.; Kim, K. S.; Yun, S. H.; Hahn, S. K. *ACS nano*, **2014**, *8*, 260.

[89] Kim, Y. C.; Park, J. H.; Prausnitz, M. R. *Adv. Drug. Deliv. Rev.*, **2012**, *64*, 1547.

[90] Lee, K.; Lee, H. C.; Lee, D. S.; Jung, H. *Adv. Mater.*, **2010**, *22*, 483.

[91] Carey, J. B.; Pearson, F. E.; Vrdoljak, A.; McGrath, M. G.; Crean, A. M.; Walsh, P. T.; Doody, T.; O'Mahony, C.; Hill, A. V.; Moore, A. C. *PLoS One*, **2011**, *6*, e22442.

[92] Ding, Z.; Verbaan, F. J.; Bivas-Benita, M.; Bungener, L.; Huckriede, A.; van den Berg, D.J.; Kersten, G.; Bouwstra, J. A. *J. Control. Release*, **2009**, *136*, 71.

[93] Li, W. Z.; Huo, M. R.; Zhou, J. P.; Zhou, Y. Q.; Hao, B. H.; Liu, T.; Zhang, Y. *Int. J. Pharm.*, **2010**, *389*, 122.

[94] Gill, H. S.; Prausnitz, M. R. *J. Control. Release*, **2007**, *117*, 227.

[95] DeMuth, P. C.; Li, A. V.; Abbink, P.; Liu, J.; Li, H.; Stanley, K. A.; Smith, K. M.; Lavine, C. L.; Seaman, M. S.; Kramer, J. A.; Miller, A. D.; Abraham, W.; Suh, H.; Elkhader, J.; Hammond, P. T.; Barouch, D. H.; Irvine, D. J. *Nat. Biotechnol.*, **2013**, *31*, 1082.

[96] Vrdoljak, A.; McGrath, M. G.; Carey, J. B.; Draper, S. J.; Hill, A. V.; O'Mahony, C.; Crean, A. M.; Moore, A. C. *J. Control. Release*, **2012**, *159*, 34.

[97] Chen, Y.; Chen, B. Z.; Wang, Q. L.; Jin, X.; Guo, X. D. *J. Control. Release*,

2017.

[98] Lee, J. W.; Park, J. H.; Prausnitz, M. R. *Biomaterials*, **2008**, *29*, 2113.

[99] Sullivan, S. P.; Koutsonanos, D. G.; Del Pilar Martin, M.; Lee, J. W.; Zarnitsyn, V.; Choi, S. O.; Murthy, N.; Compans, R. W.; Skountzou, I.; Prausnitz, M. R. *Nat. Med.*, **2010**, *16*, 915.

[100] Vrdoljak, A.; Allen, E. A.; Ferrara, F.; Temperton, N. J.; Crean, A. M.; Moore, A. C. *J. Control. Release*, **2016**, *225*, 192.

[101] Bachy, V.; Hervouet, C.; Becker, P. D.; Chorro, L.; Carlin, L. M.; Herath, S.; Papagatsias, T.; Barbaroux, J. B.; Oh, S. J.; Benlahrech, A.; Athanasopoulos, T.; Dickson, G.; Patterson, S.; Kwon, S. Y.; Geissmann, F.; Klavinskis, L. S. *Proc. Natl. Acad. Sci. USA*, **2013**, *110*, 3041.

[102] Korkmaz, E.; Friedrich, E. E.; Ramadan, M. H.; Erdos, G.; Mathers, A. R.; Ozdoganlar, O. B.; Washburn, N. R.; Falo, Jr., L.D. *J. Pharm. Sci.*, **2016**, *105*, 3453.

[103] Zhu, Z.; Ye, X.; Ku, Z.; Liu, Q.; Shen, C.; Luo, H.; Luan, H.; Zhang, C.; Tian, S.; Lim, C.; Huang, Z.; Wang, H. *J. Control. Release*, **2016**, *243*, 291.

[104] Vazquez, P.; Herzog, G.; O'Mahony, C.; O'Brien, J.; Scully, J.; Blake, A.; O'Mathuna, C.; Galvin, P. *Sens. Actuators, B*, **2014**, *201*, 572.

[105] Dul, M.; Stefanidou, M.; Porta, P.; Serve, J.; O'Mahony, C.; Malissen, B.;

Henri, S.; Levin, Y.; Kochba, E.; Wong, F. S.; Dayan, C.; Coulman, S. A.; Birchall, J. C. *J. Control. Release*, **2017**.

[106] Schipper, P.; van der Maaden, K.; Romeijn, S.; Oomens, C.; Kersten, G.; Jiskoot, W.; Bouwstra, J. *J. Control. Release*, **2016**, *242*, 141.

[107] Jun, H.; Han, M. R.; Kang, N. G.; Park, J. H.; Park, J. H. *J. Control. Release*, **2015**, *207*, 1.

[108] Yu, J.; Zhang, Y.; Ye, Y.; DiSanto, R.; Sun, W.; Ranson, D.; Ligler, F. S.; Buse, J. B.; Gu, Z. *Proc. Natl. Acad. Sci. USA*, **2015**, *112*, 8260.

[109] Ye, Y.; Yu, J.; Wang, C.; Nguyen, N. Y.; Walker, G. M.; Buse, J. B.; Gu, Z. *Adv. Mater.*, **2016**, *28*, 3115.

[110] Heikenfeld, J. *Nature* **2016**, *529*, 475.

[111] Bandodkar, A. J.; Jia, W.; Yardimci, C.; Wang, X.; Ramirez, J.; Wang, J. *Anal. Chem.*, **2015**, *87*, 394.

[112] Lee, H.; Choi, T. K.; Lee, Y. B.; Cho, H. R.; Ghaffari, R.; Wang, L.; Choi, H. J.; Chung, T. D.; Lu, N.; Hyeon, T.; Choi, S. H.; Kim, D.-H. *Nat. Nanotech.*, **2016**, *11*, 566.

[113] Lee, H.; Song, C.; Hong, Y. S.; Kim, M. S.; Cho, H. R.; Kang, T.; Shin, K.; Choi, S. H.; Hyeon, T.; Kim, D.-H. *Sci. Adv.*, **2017**, *3*, e1601314.

[114] Koh, A.; Kang, D.; Xue, Y.; Lee, S.; Pielak, R. M.; Kim, J.; Hwang, T.; Min, S.; Banks, A.; Bastien, P. *Sci. Transl. Med.*, **2016**, *8*, 366ra165.

[115] Choi, J.; Kang, D.; Han, S.; Kim, S. B.; Rogers, J. A. *Adv. Healthc. Mater.*, **2017**, *6*.

[116] Moyer, J.; Wilson, D.; Finkelshtein, I.; Wong, B.; Potts, R. *Diabetes. Technol. Ther.*, **2012**, *14*, 398.

Chapter 2. Temperature-responsive Transdermal Drug Delivery Devices for Treatment of Diabetes

2.1 Introduction

Transdermal drug delivery has attracted a growing attention, due to its convenience and less painful procedure than direct injection.[1-4] Since early 1970s, various drugs which are delivered by transdermal routes have been commercialized.[5] However, only hydrophobic and low molecular-weight drugs can be transported through skin. To broaden the variety of transdermal drugs, disruption of skin layers with microneedles has been investigated for enhanced transdermal drug delivery. Recently, smart microneedle systems havebeen studied for treatment of various diseases including tumor and diabetes.[6-8]

Diabetes has been on the rise every year, and the control of blood glucose level is of great concern for diabetes. Metformin is one of the first-line drugs for treating type 2 diabetes.[9,10] However, it requires high

dose and can cause gastric problems. Since drug delivery through the skin can bypass the digestive system, much lower drug dosage would be needed for delivering metformin transdermally, while preventing gastrointestinal side effects. Moreover, precise maintenance of homeostasis through controlled drug delivery would be possible, which is highly desirable for diabetes.[11]

In this chapter, I describe the development of precisely controlled multi-stage transdermal drug delivery system for type 2 diabetes (**Figure 2.1**), which is made of thermos-sensitive microneedles and flexible heaters (**Figure 2.2**). Drugs for the transdermal therapy are loaded on two different temperature-responsive phase change nanoparticles (PCNs). These nanoparticles are embedded in hyaluronic acid hydrogel microneedles, which are additionally coated with biocompatible phase change material. This system enables multi-stage, spatially patterned, and precisely controlled drug release with integrated flexible heaters.

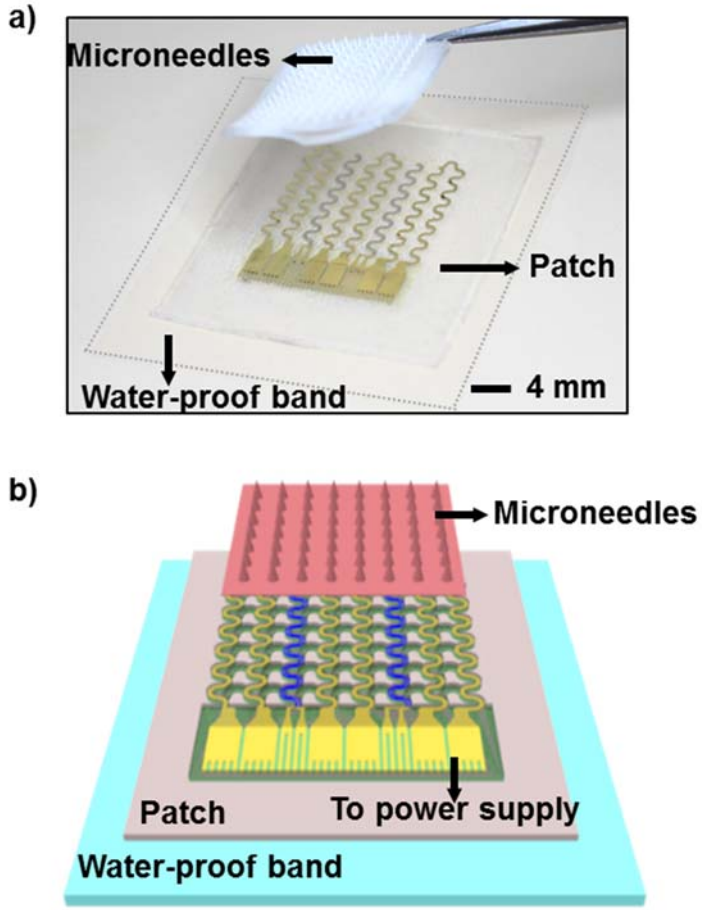

Figure 2.1. Integrated transdermal drug delivery device. (a) Optical camera image (dotted line: edges of the patch) and (b) schematic illustration of the transdermal drug delivery device. Replacement-type microneedles are assembled on a three-channel thermal actuator.

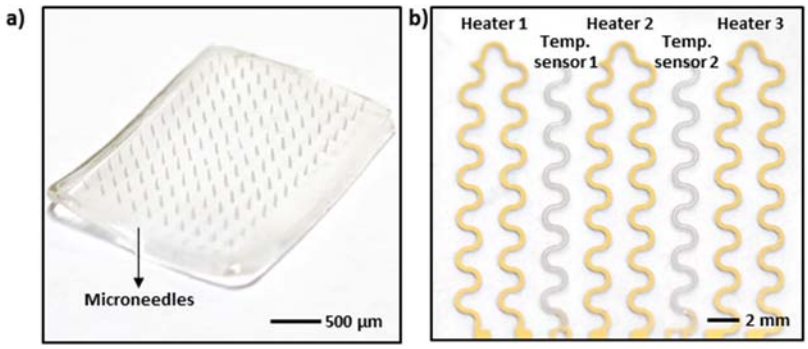

Figure 2.2. Optical camera image of transdermal drug delivery device. (a) Optical camera image of thermo-responsive and bioresorbable microneedles. (b) Optical camera image of a transdermal drug delivery device before integrating the microneedles.

2.2 Experimental Section

2.2.1 Synthesis procedure and characterization of phase change nanoparticles

0.5 g of PCM for PCN1 (palm oil; Product #70905, Sigma-Aldrich, USA) or PCN2 (tridecanoic acid; Product #T0412, Tokyo Chemical Industry, Japan), 0.03 g of F127 (Product #P2443, Sigma-Aldrich, USA), 0.02 g of DOPA-conjugated hyaluronic acid, and metformin (Product #D150959, Sigma-Aldrich, USA) or chlorpropamide (Product #C129531, Aladdin, USA) are dissolved in water. In case of the releasing test, rhodamine B dye is added to the solution to visualize and analyze the loading and releasing of drugs into and from PCNs in the microneedle matrix. The solution is sonicated for 30 min with a probe-type ultra-sonicator.

The nuclear magnetic resonance (NMR) data of HA and DOPA-conjugated HA are obtained using Avance-500 (Bruker) at National Center for Inter University Research Facilities (NCIRF). PCN1 and PCN2 are observed by cryo-TEM and TEM. The hydro-diameter and zeta potential of PCNs are measured at skin temperature (30 °C) and drug

delivery temperatures (40 °C, 45 °C) by Zetasizer Nano S90. Dye release from the PCNs is measured with a photoluminescence spectrometer (λ_{em}: 570 nm) while changing the temperature from 30 °C (skin temperature) to 45 °C (drug-release temperature).

2.2.2 Fabrication of microneedles

A female polydimethylsiloxane (Sylgard 184, Dow chemical, USA) mold is prepared based on commercial microneedles (PAMAS, Prestige, Republic of Korea). The microneedles have a height of 1 mm and a round base diameter of 250 μm. The drug-loaded PCNs (metformin; Product #D150959, Sigma-Aldrich, USA or chlorpropamide; Product #C129531, Aladdin, USA) and a 2 % hyaluronic acid solution are casted on the PDMS mold. The sample is placed under vacuum until no bubble is generated. After degassing, the sample is dried at room temperature. The microneedles are carefully peeled from the mold. The PCM (tetradecanol; Product #185388, Sigma-Aldrich, USA) is sprayed on the microneedles. The morphology of the microneedles is examined with a field emission scanning electron microscope.

2.2.3 *In vitro* characterization of microneedles

Dissolution of PCM-coated and PCM-uncoated microneedles is tested in the PBS. The rigidity of the microneedles is measured with the universal testing machine (maximum weight: 10 N, scan rate: 0.1 mm s^{-1}). To observe the penetration of the microneedles, a tissue-like 4 % agarose gel is used, and the penetration is examined by a confocal laser fluorescence microscope. Thermal actuation by the heater and the corresponding dye release into the agarose gel are imaged by an IR camera (FLIR E8, FLIR, USA) and a confocal laser fluorescence microscope. The dye-release profile of the PCM-coated microneedles is measured during the temperature change from 30 °C (skin temperature) to 45 °C (drug-release temperature). The multi-stage dye release with the three-channel thermal actuation is measured by the photoluminescence spectrometer (λ_{em}: 570 nm). In the case of the hot weather, external temperature can reach beyond the transition temperature. In this condition, other phase change materials (PCMs) can be used for a higher melting temperature.

2.2.4 *In vivo* characterization of microneedles

In vivo experiment of the microneedles is conducted using 8-to-12-week-old db/db mice. All mice were fasted overnight before the experiment.

The drug-loaded microneedles are attached to the shaved abdomen skin of the db/db mouse with a gentle pressure. The transcutaneous drug delivery is started with the thermal actuation by the embedded heater. The change in the blood glucose levels is measured using a commercial glucose meter (Accu-chek performa, Roche, Switzerland).

2.2.5 Ethical approval for the animal experiment

All procedures are approved by the Institutional Animal Care and Use Committee (IACUC) of the Biomedical Research Institute of Seoul National University Hospital. All experiments are performed according to IACUC guide.

2.3 Result and Discussion

2.3.1 Thermo-responsive phase change nanoparticles

Phase change materials (PCMs) have low melting temperatures but above human body temperature, and thus they are widely used in the thermo-responsive drug delivery. Phase change nanoparticles (PCNs) are made of PCMs, drugs, and biocompatible ligands (**Figure 2.3**). Different PCNs enable temperature-dependent step-wise drug delivery. We use palm oil (PCN1, T_m: 38 °C) and tridecanoic acid (PCN2, T_m: 43 °C), which melt above the skin temperature (30 °C; fig. S9A). The drugs (metformin or chlorpropamide) are embedded in the PCM matrix (Fig. 3A and figs. S9B-D). Pluronic F127 and 3,4-dihydroxyl-L-phyenylalanine (DOPA)-conjugated hyaluronic acid (**Figure 2.4**) are used as ligands, which make an oil-in-water (o/w) emulsion. Cryo-transmission electron microscopy (cryo-TEM) images show that PCNs below the melting temperature are solid. Above the melting temperature, PCNs change to liquid and aggregate (**Figure 2.5**). Cytotoxicity tests show that both PCNs are non-toxic and suitable for biomedical applications (**Figure 2.6a**). The hydrodynamic diameters and negative

zeta potentials of the PCNs slightly increase and decrease, respectively, as the temperature increases from skin temperature (30 °C; **Figure 2.6b**) to above melting temperatures (40 °C and 45 °C; **Figures 2.6c and 2.6d**). The PCM matrices can block the drug release before thermal actuation. Their step-wise temperature-dependent melting controls the amount of the drug release. When the temperature reaches 40 °C, only the drugs contained in PCN1 is released, while at 45 °C, drugs in both PCN1 and PCN2 are released (**Figure 2.6e**).

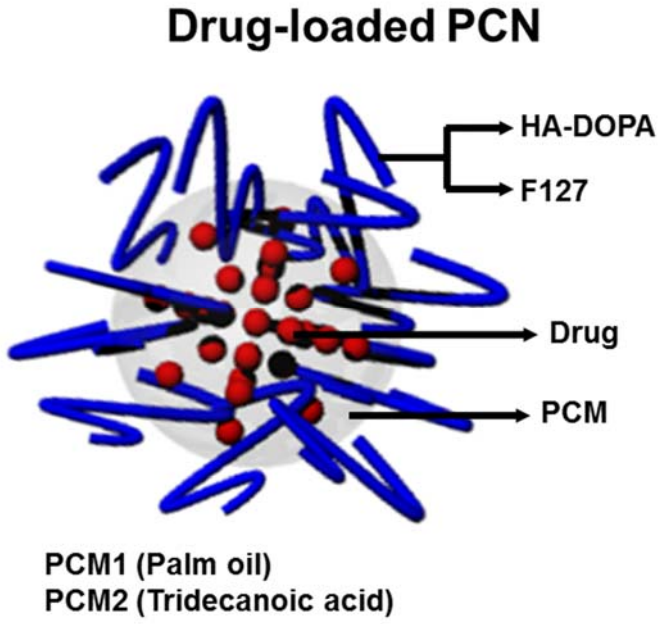

Figure 2.3. Schematic illustration of the phase change nanoparticle.

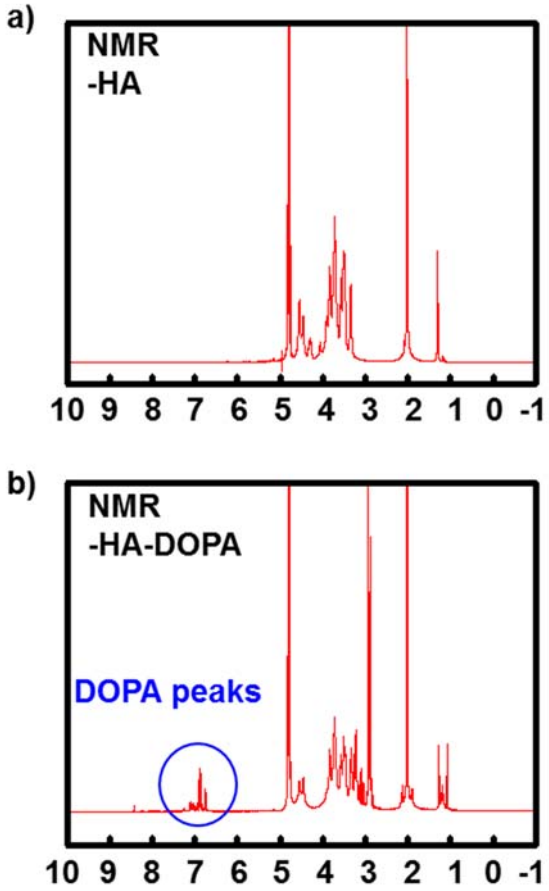

Figure 2.4. Characterization of hyaluronic acid, DOPA-conjugated hyaluronic acid. (a) Nuclear magnetic resonance analysis data of hyaluronic acid. (b) Nuclear magnetic resonance analysis data of DOPA-conjugated hyaluronic acid

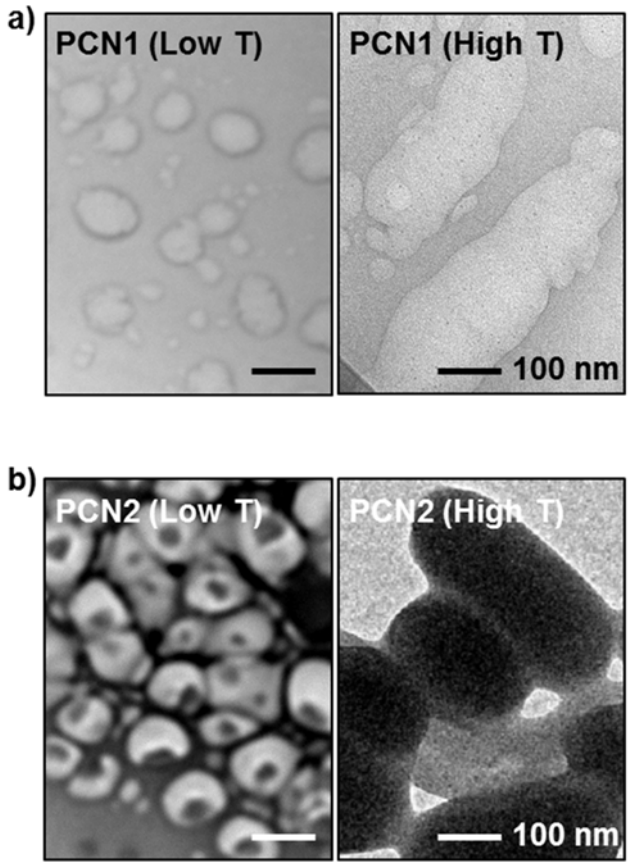

Figure 2.5. TEM images of PCNs. (a) Cryo-TEM image of PCN1 (palm oil) below the melting temperature (left) and TEM image of PCN1 above the melting temperature (right). (b) Cryo-TEM image of PCN2 (tridecanoic acid) below the melting temperature (left) and TEM image of PCN2 above the melting temperature (right).

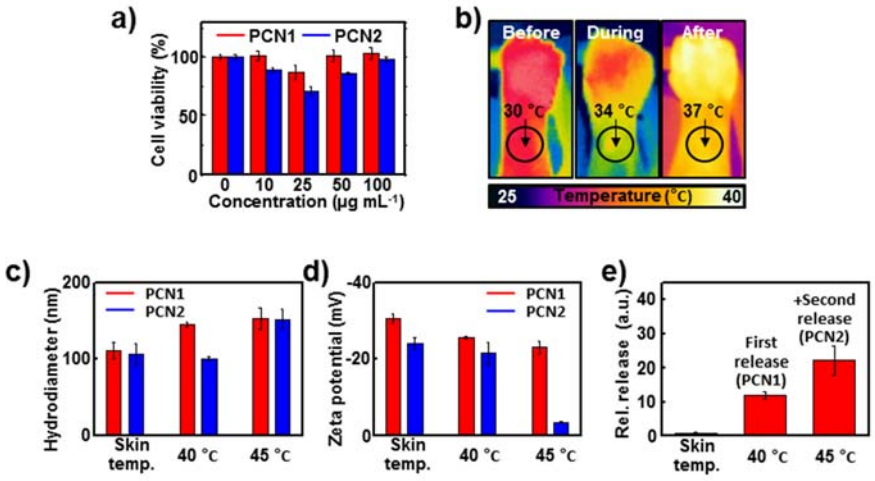

Figure 2.6. Characterization of the phase change nanoparticles. (a) Cell viability test at different concentrations of PCNs (4 h exposure). (b) IR camera image of the human skin before, during, and after exercise. (c) Dynamic light scattering size measurement of PCNs at 30 (skin temperature), 40, and 45 °C. (d) Zeta potential measurement of PCNs at 30 (skin temperature), 40, and 45 °C. (e) Step-wise drug delivery of PCNs at 30 (skin temperature), 40, and 45 °C.

2.3.2 Microneedles fabrication and characterization

The microneedles are fabricated by molding the hyaluronic acid hydrogel matrix containing drug-loaded PCNs followed by an additional PCM spray coating (**Figure 2.7**). SEM and optical images confirm that PCM-coated microneedles are made (**Figures 2.8a and 2.8b**). A confocal laser fluorescent microscopy image shows that the dye-loaded PCNs are well-embedded in the microneedles (**Figure 2.8c**). Hydrogel-based microneedles dissolve when they come in contact with body fluids, while the PCM coating prevents the dissolution before the controlled melting of the PCM (**Figure 2.9a**). The microneedles should be stiff enough to penetrate into the skin; compression tests confirm their mechanical strength (**Figure 2.9b**). The microneedles successfully penetrate into 4 % agarose gel (tissue-like gel) and generate pores (**Figure 2.10a**). After poration by microneedles, vertical heat transfer dissolves the outside PCM coating and embedded PCNs. Although accidental peel-offs create small defects in the PCM coating, the drug contained in the PCNs is not released. The vertical temperature distribution of the agarose gel imaged by an infrared (IR) camera confirms the successful heat transfer (**Figure 2.10b**).

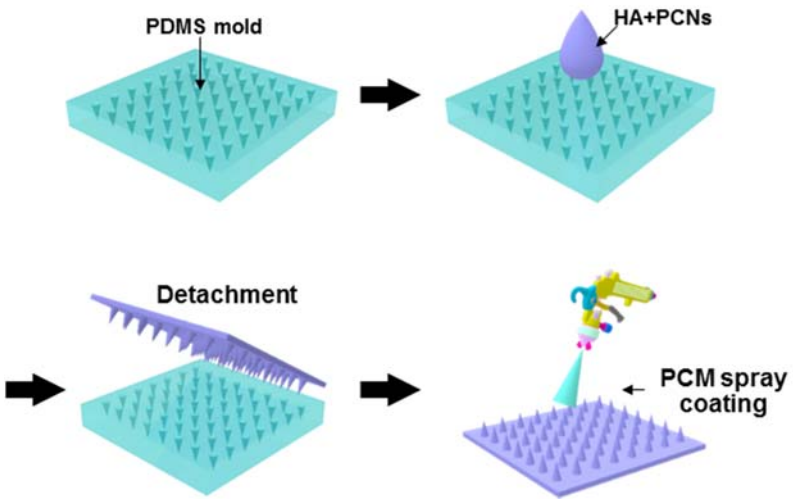

Figure 2.7. Fabrication process of the microneedles. Schematic illustration of the fabrication process of the microneedles. Microneedles are made of two types of drug-loaded PCNs and a hyaluronic acid matrix. They are coated with a biocompatible PCM after detaching from the mold.

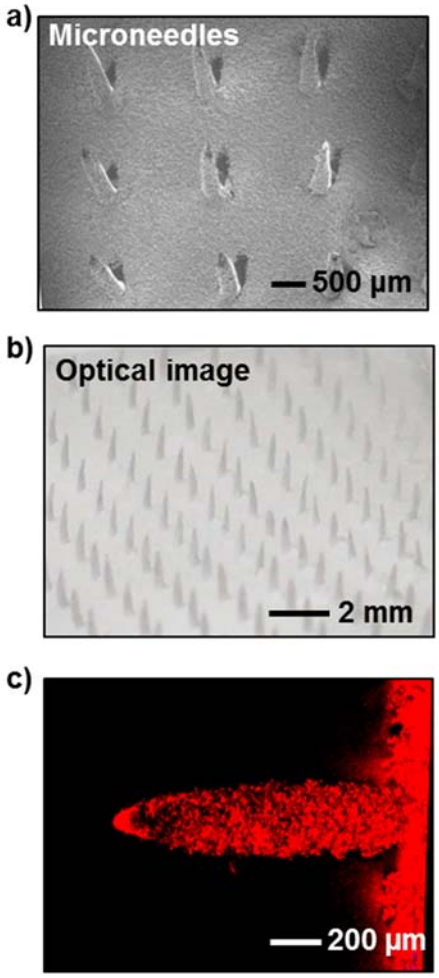

Figure 2.8. . (a) SEM image and (b) Optical image of PCM-coated microneedles (c) confocal microscope image of microneedles with dye-loaded PCNs.

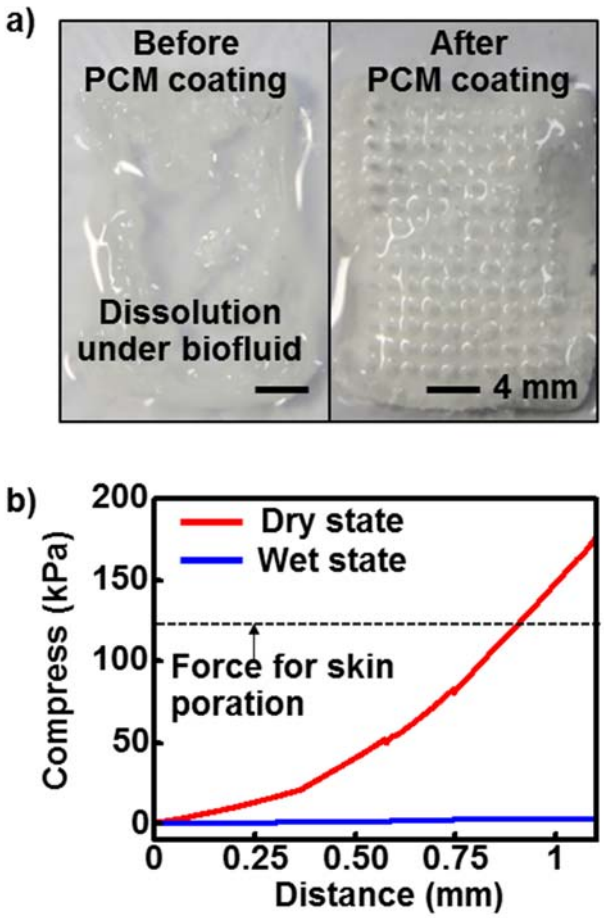

Figure 2.9. Characterization of microneedles. (a) Microneedle dissolution test in PBS before (left) and after the PCM coating (right). (b) Mechanical strength test of microneedles in their dry and wet states.

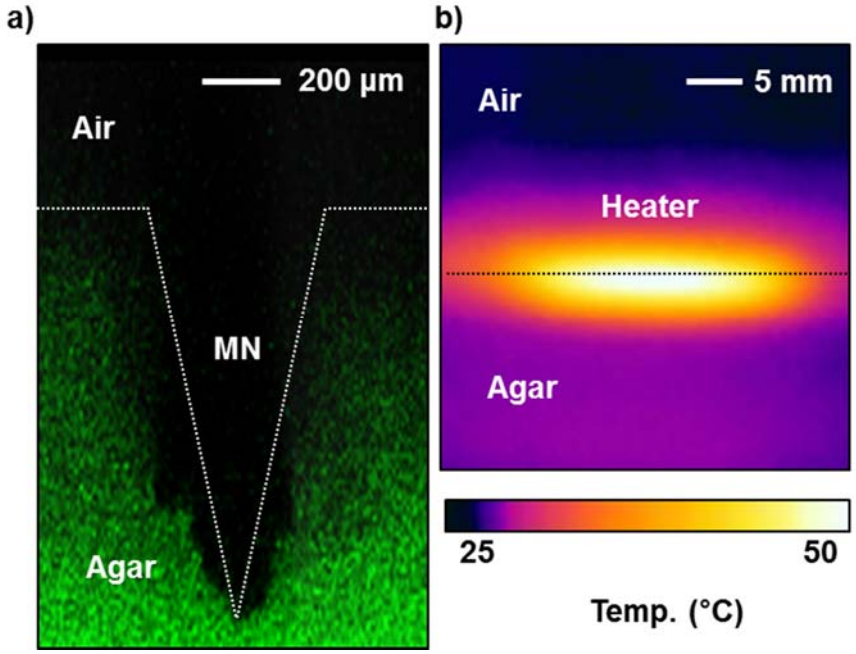

Figure 2.10. (a**)** Confocal microscope image of microneedles penetrating into 4 % agarose gel. (b) IR camera image of the thermal actuation on the gel.

2.3.3 Multi-stage drug delivery

There is a negligible release under and around skin temperature (30 ^{o}C) due to the PCM coating and PCNs. At the elevated temperature (40 °C), the PCM coating and PCN1 are dissolved, and metformin in PCN1 are released. At the higher temperature (45 °C), metformin in both PCN1 and PCN2 are released (**Figure 2.11**). To investigate the step-wise drug release, microneedles containing dyes are heated from 25 °C to 45 °C (**Figure 2.12**). Spatial patterning of the embedded heater subdivides the release steps further, which is precisely controlled by co-integrated temperature sensors (**Figure 2.13**). Heaters consisting of three channels together with the two types of PCNs result in eight different spatio-thermal patterns (**Figure 2.14a**) and six-stage programmed dye-release profiles (**Figure 2.14b**).

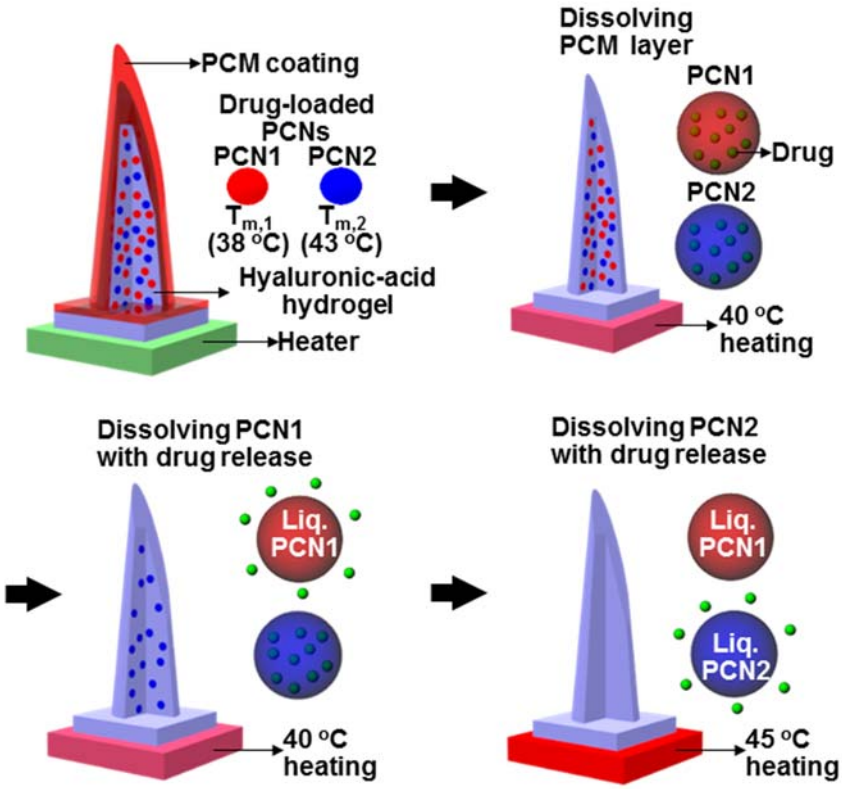

Figure 2.11. Drug delivery from microneedles with integrated heaters. Drug release from microneedles can be controlled by stepwise thermal actuation of integrated heater.

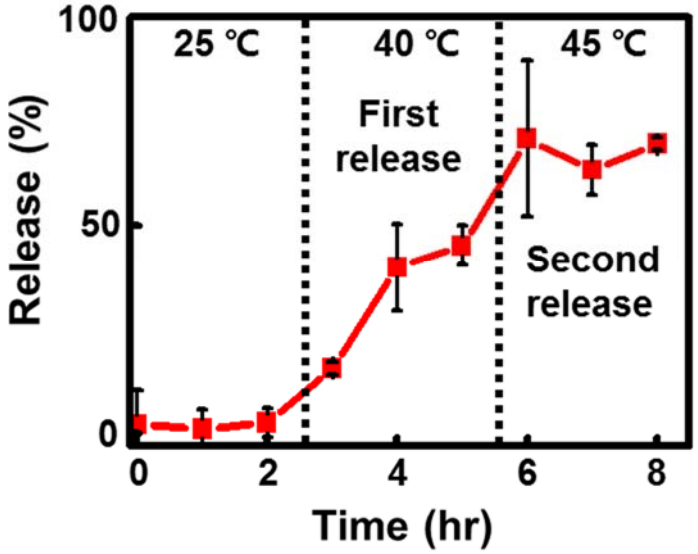

Figure 2.12. Controlled drug-release profile from microneedles.

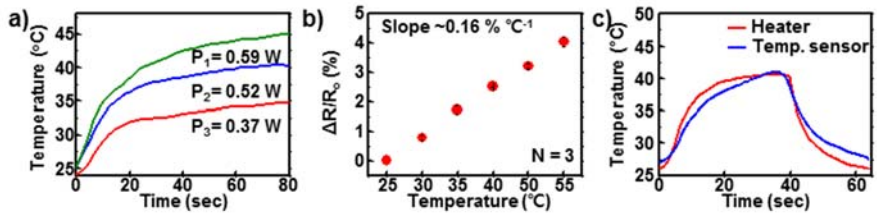

Figure 2.13. Characterization of the heater and temperature sensor and their co-operation. (a) Output temperature profiles of the heater at different powers (P_1-P_3). (b) Characterization of the temperature sensor. (c) *In situ* temperature monitoring of the heater by using a commercial IR camera and the integrated temperature sensor.

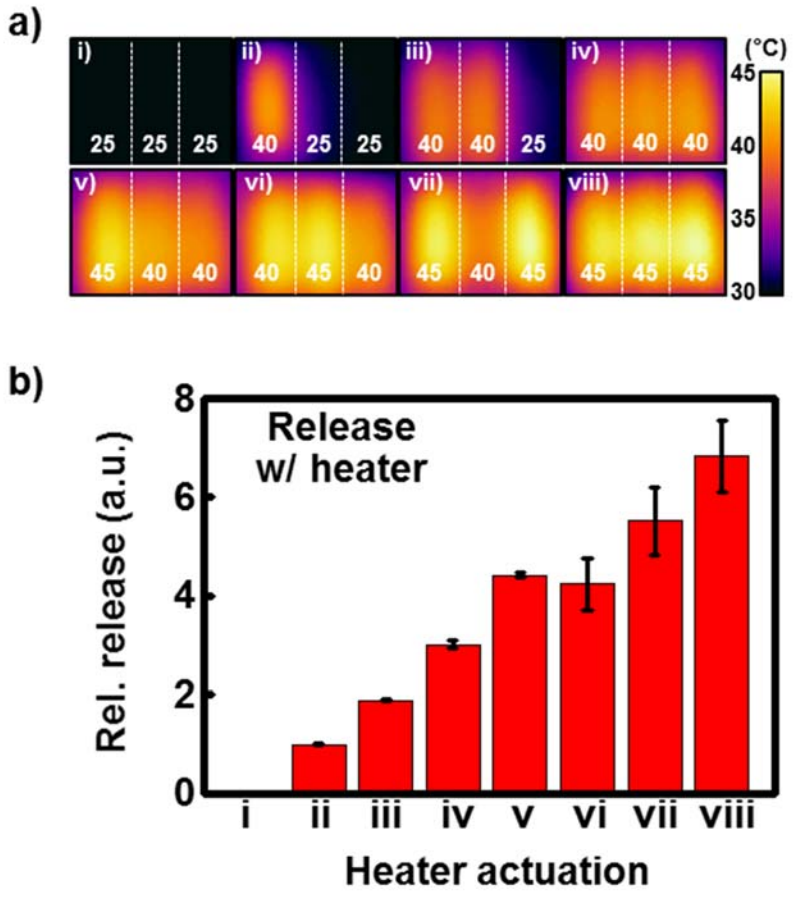

Figure 2.14. Multi-stage drug delivery module. (a) IR camera images of eight different spatio-thermal profiles by using the three-channel thermal actuator for multi-stage drug delivery. (b) Multi-stage drug-release profile.

2.3.4 Controlled transdermal drug delivery using microneedles

Transdermal drug delivery experiments based on the fabricated microneedles and integrated heaters *in vivo* are conducted on 8-to-12-week-old diabetic (db/db) mice (type 2 diabetes mellitus model). The *in vivo* treatment starts with lamination of a therapeutic patch on the shaved abdomen of the db/db mouse (**Figure 2.15a**). Trypan blue staining on the mouse skin confirms that the microneedles can successfully penetrate the skin for the drug (metformin) delivery (**Figure 2.15b**). The integrated heaters modulate the amount of the drug delivery by the controlled thermal actuation (**Figure 2.16a**). Control groups that have no patch (black), microneedles without diabetes drugs (red), and microneedles with diabetes drugs (blue: dose 1, green: dose 2) are used (**Figure 2.16b**). The experimental groups (blue and green) show significant decrease in the blood glucose level in comparison to the control groups (black and red). As more metformin is delivered to the db/db mice, the blood glucose level is suppressed more. The blood glucose concentration of the measurement group (dose 2: green) decreased to 7.6 mM, which is a normoglycemic state (< 11 mM).

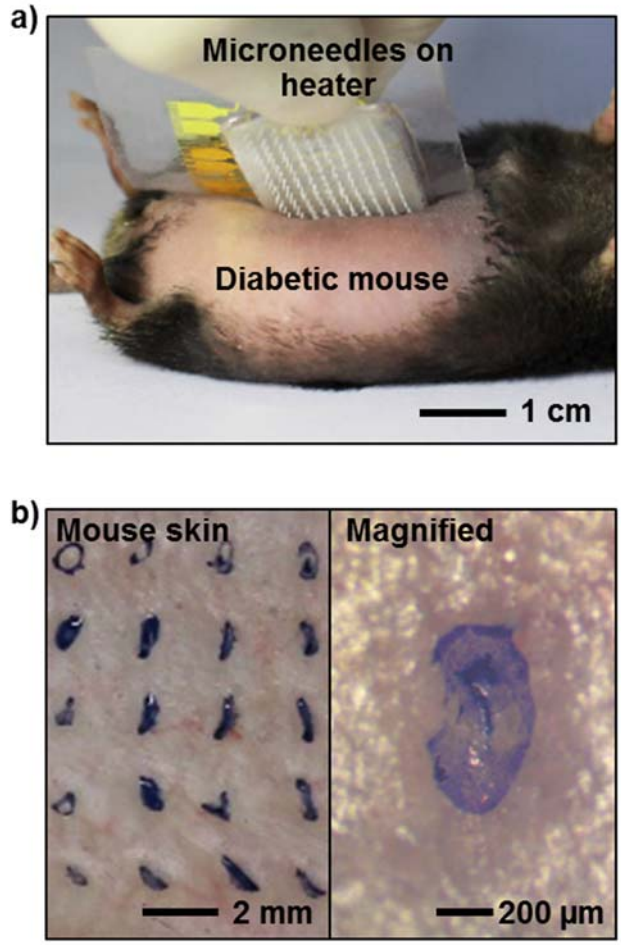

Figure 2.15. *In vivo* microneedles therapy. (a) Optical camera image of the transdermal drug delivery device on the db/db mouse. (b) Optical camera images of the mouse skin with the trypan blue staining (left) and its magnified view (right).

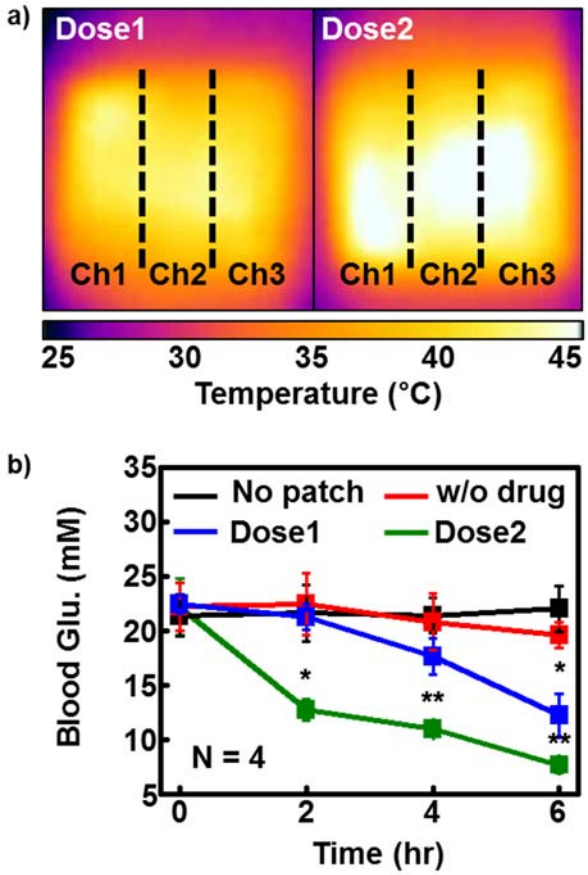

Figure 2.16. *In vivo* microneedles therapy. (a) IR camera images of the thermal actuation for the transdermal drug delivery (dose1: 40 °C, dose2: 45 °C). (b) Blood glucose levels of the db/db mice for the treated groups (microneedles with the drugs) and control groups (without the patch, microneedle without the drugs) (*$P < 0.05$, **$P < 0.01$ versus control, Student's t-test).

2.4 Conclusion

I report a novel microneedle system for the treatment of type 2 diabetes. The system can reduce the stress of repetitive insulin shots and lower the dose of diabetes drugs. For highly controlled drug delivery, the microneedles are coated with phase change materials, and the drugs are loaded in two kinds of phase change nanoparticles. Three-channel heaters and the developed microneedles enable multi-stage drug delivery up to six modules. This smart microneedle system enables the precise control of blood glucose levels and provides a patient-friendly way to treat the diabetes mellitus.

Most of the contents in this chapter were published in the article, "Wearable/disposable Sweat-based Glucose Monitoring Device with Multistage Transdermal Drug Delivery Module." (*Science Advances* **2016, *3*, e1601314)

2.5 References

[1] Prausnitz, M. R.; Langer, R. *Nature Biotech.* **2008**, *26*, 1261.

[2] Prausnitz, M. R. Microneedles for transdermal drug delivery. *Adv. Drug Deliv. Rev.* **2004**, *56*, 581.

[3] Prausnitz, M. R.; Mitragotri, S.; Langer, R. *Nat. Rev. Drug. Discov.*, **2004**, *3*, 115.

[4] Lee, J. W.; Gadiraju, P.; Park, J. H.; Allen, M. G.; Prausnitz, M. R. *J. Control. Release*, **2011**, *154*, 58.

[5] D.W. Sifton, *Medical Economics/Thomson Healthcare* **2002**.

[6] Yu, J.; Zhang, Y.; Ye, Y.; DiSanto, R.; Sun, W.; Ranson, D.; Ligler, F. S.; Buse, J. B.; Gu, Z. *Proc. Natl. Acad. Sci.* **2015**, *112*, 8260-8265.

[7] Wang, C.; Ye, Y.; Hochu, G. M.; Sadeghifar, H.; Gu, Z. *Nano. Lett.*, **2016**, *16*, 2334.

[8] Di, J.; Yao, S.; Ye, Y.; Cui, Z.; Yu, J.; Ghosh, T. K.; Zhu, Y.; Gu, Z. *ACS nano*, **2015**, *9*, 9407

[9] UKPDS Group, *Lancet* **1998**, *352*, 854.

[10] Sambol, N. C.; Chiang, J.; O'Conner, M.; Liu, C. Y.; Lin, E. T.; Goodman, A. M.; Benet, L. Z.; Karam, J. H. *J. Clin. Pharmacol.* **1996**, *36*, 1012.

[11] Lee, H.; Choi, T. K.; Lee, Y. B.; Cho, H. R.; Ghaffari, R.; Wang, L.; Choi, H. J.; Chung, T. D.; Lu, N.; Hyeon, T.; Choi, S. H.; Kim, D.-H. *Nature Nanotech.* **2016**, *11*, 566.

Chapter 3. Multifunctional Theranostic Nanoparticles for Colon Cancer Treatment

3.1. Introduction

Nanomaterials have attracted great attention for their medical applications because of their size-dependent properties and unique functions. Nanoparticles can be used as drug delivery vehicles, imaging agents, and therapeutic agents.[1-7] Functional nanoparticles also enable the responsive drug delivery systems, which can reduce the side effects of drugs and act specifically on the targeted region.[8-12] For example, gold nanorods can absorb near infrared (NIR) light and generate heat for photothermal therapy.[13,14]

The gastrointestinal tract is a challenging anatomical target for diagnostic and therapeutic procedures for bleeding, polyps, and cancerous growths.[15] Advanced endoscope system that combines imaging and therapeutic functions for the gastrointestinal tract would

provide an advantage over stand-alone diagnostic or therapeutic devices. Nanoparticles are useful for the real-time imaging of tumors during the endoscopic surgery.[16] For advanced endoscopic surgery system, biocompatible theranostic nanoparticles (NPs) loaded with phototherapeutic and chemotherapeutic agents are custom-designed, which can be delivered to tumor region by active targeting.[17-20] These NPs can be activated with a light source at the tip of endoscope for fluorescence-based mapping and localized photo/chemotherapy.

In this chapter, gold nanorod@meso-porous silica core@shell particles are coated with thermosensitive poly(N-isopropylacrylamide) (PNIPAAm) to prevent doxorubicin (chemo-drugs) from being released before NIR laser irradiation. For combined therapies, photodynamic (PDT)-, photothermal (PTT)-, and chemo-therapies are induced by PDT dyes (chlorin e6; Ce6), gold nanorods (Au NRs), and chemo-drugs (doxorubicin; Dox) loaded in the mesoporous silica shell (MSS), respectively, which can effectively destroy colon cancer cells upon activation with red or NIR light irradiation.

3.2 Experimental Section

3.2.1 Synthesis of multifunctional theranostic NPs

Multifunctional theranostic NPs are synthesized by multiple stepwise reactions and separation processes. The synthetic process consists of i) Au NR synthesis, ii) MSS synthesis, iii) PDT and FL dyes conjugation, iv) PNIPAAm encapsulation, and v) antibody conjugation and Dox loading.

i) Au NR synthesis: Au seed solution is made by injecting the $NaBH_4$ solution (600 μL, 10 mM) to an aqueous seed solution containing $HAuCl_4 \cdot 3H_2O$ (250 μL, 10 mM) and cetyltrimethylammonium bromide (CTAB) (7.5 mL, 100 mM). The growth solution is made by adding $HAuCl_4 \cdot 3H_2O$ (1.7 mL, 10 mM) and $AgNO_3$ (250 μL, 10 mM) to the CTAB solution (40 mL, 100 mM), into which L-ascorbic acid (270 μL, 100 mM) is injected. This Au seed is then converted to Au NR by injecting the additional seed solution (420 μL) into a growth solution, which is left to react for 3 hours. The final product solution is centrifuged twice.

ii) MSS synthesis: The silica shell is grown on the surface of Au NR. Tetraethyl orthosilicate (TEOS) (30 μL) is injected to the Au NR solution

(50 mL) under alkaline conditions (pH 10–11) and reacted with Au NRs for 4 hours. Functionalization of the silica surface is achieved by injecting (3-aminopropyl) triethoxylsilane (10 μL) and 3-(methacryloxy) propyl triethoxysilane (10 μL) and the solution is stirred for 4 hours. Then, the silica-coated Au NRs are centrifuged twice and dispersed in the ethanol. To create pores in the silica shell, HCl is added to the NP-ethanol suspension to adjust its pH to 1–2, which is refluxed to remove the CTAB templates. The resulting Au NR@MSS is centrifuged twice and dispersed in water.

iii) PDT and FL dyes conjugation: Chlorin e6 (Ce6) reacts with the equimolar amount of N-(3-dimethylaminopropyl)-N'-ethylcarbodiimide hydrochloride (EDC) and N-hydroxysuccinimide (NHS). And the functionalized chlorine e6 is reacted with AuNR@MSS for 12 hours. To conjugate FL dyes, Rhodamine B isothiocyanate are mixed and reacted for 12 hours. After the conjugation, AuNR@MSS is centrifuged and dispersed in water.

iv) PNIPAAm encapsulation: In order to produce a PNIPAAm shell, the Au NR@MSS solution (5 mL) is reacted with N-isopropylacrylamide (NIPAAm) (12 mL, 100 mM), acrylic acids (1.4 mL, 100 mM), N, N'-methylenebis(acrylamide) (1.2 mL, 100 mM), acrylate-PEG-NHS (20

mg), sodium dodecyl sulfate (200 μL). The solution is bubbled with argon and heated to 70 °C to remove oxygen. After 30 min, potassium persulfate (1 mL, 20 mM) is injected to initiate the polymerization. The Au NR@MSS@PNIPAAm solution is then centrifuged twice to remove unreacted chemical regents.

v) Antibody conjugation and Dox loading: The cetuximab (antibody) (2 mL, 5 mg/mL) is added to the Au NR@MSS@PNIPAAm solution for the conjugation. The NHS-end group is reactive with the PEG-end group. This antibody-conjugated Au NR@MSS@PNIPAAm is then centrifuged and dispersed in PBS. Then, Dox (1 mL, 0.6 mg/mL) solution is added to the NPs solution (5 mL) and stirred for one day. Excess Dox is removed by centrifuging NPs.

3.2.2 Characterization of theranostic NPs

The size changes of the synthesized NPs according to the temperature change (increase from 20 to 55 °C and decrease from 55 to 20 °C) are measured by the dynamic light scattering. The hydrodynamic diameter is measured for every 5 °C increment. Temperature changes in the Au NR and PBS solution (concentration of 50, 100 and 200 μg/mL) induced

by the CW NIR laser irradiation (1 W, 5 min) are measured by the IR camera at 0, 1, 2, 3, 4 and 5 min. UV-vis spectrophotometry is used to calculate the amount of drug loaded on NPs by measuring the initial and supernatant Dox peak intensity values at 480 nm. Photoluminescence spectrophotometry is used to acquire the amount of released drug by measuring supernatant Dox peak intensity value at 580 nm (excitation wavelength of 480 nm). Florescence correlation spectroscopy (FCS) is used to calculate the amount of conjugated FL dyes on NPs. The amount of PDT dyes conjugated on NPs is measured by using UV-vis spectrophotometer and ICP-AES (Inductively coupled plasma atomic emission spectroscopy).

3.2.3 Preparation of FHC and HT-29 for *in-vitro* experiments

Human colon epithelial normal cells (FHC) were purchased from ATCC (catalogue number: CRL-1831) and human colon epithelial cancer cells (HT-29) were purchased from Korean Cell Line Bank (catalogue number: 30038). The culture medium for the FHC (ATCC, CRL-1831) is DMEM/F-12 (Life technologies, 11320) with 10 % bovine serum (Life technologies, 16000), 1 % penicillin streptomycin, 25 mM HEPES, 10 ng/mL cholera toxin, 5 μg/mL insulin, 5 μg/mL transferrin,

and 100 ng/mL hydrocortisone. The culture medium for the HT-29 (KCLB, 30038) is RPMI1640 containing 10 % bovine serum and 1 % penicillin streptomycin. Both cell types are deposited on culture plates and incubated at 37 °C under the atmosphere of 5 % CO_2.

3.2.4 Cytotoxicity evaluation and *in-vitro* active targeting efficiency of NPs

The cytotoxicity of the NPs is measured by MTS assay, in which HT-29 cells are suspended in the culture medium with a concentration of 1×10^5 cells/mL. The 100 μL of this suspension is dispensed in each well of a 96 well plate. After the incubation for 2 days, Dox-loaded and unloaded NPs with the PNIPAAm encapsulation as well as Dox-loaded NPs without the PNIPAAm encapsulation are injected to check the cytotoxicity. After 1 day, each cell is washed and 100 μL of the fresh cell culture medium is added along with 20 μL of the MTS solution (CellTiter 96 AQ_{ueous}). After the further incubation for 2 hours, the light absorbance at 490 nm, which is proportional to the cell viability, is measured by a cell plate reader. To estimate the active targeting efficiency, NPs are injected into the FHC and HT-29 cell media. Cells are incubated for 4 hours and washed twice to remove remaining NPs. Since NPs are

conjugated with a red fluorescence dye (RITC), their active targeting efficiency can be characterized by the red fluorescence mapping ($\lambda_{ex}/\lambda_{em}$=550/580 nm) using the confocal laser scanning microscopy (CLSM). The cell nuclei are also dyed with DAPI (4',6-diamidino-2-phenylindole) to identify the location of individual cells ($\lambda_{ex}/\lambda_{em}$=340/488 nm). The uptake of NPs by FHC and HT-29 is measured by a flow cytometer, in which 10,000 cells are counted. The targeting efficiency of free Ce6 and Ce6-conjugated NPs is also compared. ROS generation after irradiation of CW red laser is measured with ROS sensing dye (DHR123, $\lambda_{ex}/\lambda_{em}$=488/520 nm) using CLSM.

3.2.5 *In-vitro* photo-therapy experiments using theranostic NPs

The therapeutic effect of NPs is estimated by treating HT-29 cells with NPs which are not conjugated with RITC, incubating cells for 4 hours, and then washing them twice to remove remaining NPs. In the case of PTT, NPs without the Dox loading are used. For the chemotherapy, Dox-loaded NPs are used. A pulsed laser (wavelength 690 nm, power 0 mW to 40 mW for PDT; wavelength 808 nm, power 0 mW to 40 mW for PTT) is used and irradiated for 10 min. 10 μL of calcein AM (1 mg/mL) and propidium iodide (1 mg/mL) are added afterwards. CLSM is used to

measure the cell viability based on the excitation/emission wavelengths of calcein AM ($\lambda_{ex}/\lambda_{em}$=488/520 nm) and propidium iodide ($\lambda_{ex}/\lambda_{em}$=550/620 nm**)**.

3.2.6 Animal experiment and related animal model of HT-29 cancer

All procedures are approved by the Institutional Animal Care and Use Committee (IACUC) of the Biomedical Research Institute of Seoul National University Hospital, and all experimental procedures are performed according to the IACUC guidelines. HT-29 cancer cells (1×10^6) in 50 μL of serum-free media are mixed with an equivalent volume of Matrigel (BD Biosciences). The mixture is subcutaneously injected into the flank of female BALB/c-nude mouse (aged 6-8 weeks). All experiments are performed when the size of tumor is 100 ± 30 mm^3 (2 weeks after the tumor implantation). After photo therapies, the mice are divided into two groups. One group is monitored to check the efficacy of treatment. The size of tumors is checked every three days and the mice are sacrificed 20 days after the treatment. The mice in the other group are killed at 7 days post treatment and used for immunohistochemistry.

3.2.7 *In-vivo* toxicity, active targeting, and photo-therapies of NPs.

NPs are intravenously injected into the BALB/c-nude mouse model with colon cancer through the tail vein. The estimation of *in-vivo* toxicity is based on histology analysis of the organs. Individual organs show no inflammations after NPs targeting. The tumor targeting efficiency of NPs is characterized through pharmacokinetics, biodistribution and fluorescence studies. Blood samples are collected at 10 min, 30 min, 2 hours, 6 hours, 24 hours after the NP injection. After 24 hours, the mice are sacrificed and the organs are collected for quantitative measurement of NPs distribution. The collected blood and organ samples are dissolved by the acid solution and the Au concentration is measured by ICP-MS. The fluorescent images of the whole body and the extracted organs are obtained using IVIS Lumina II (PerkinElmer). *In-vivo* photo- and chemo- therapies using NPs are performed with the radiation of red and NIR CW lasers. The tumor region is irradiated by 670 nm-red laser (500 mW for 6 min) for PDT or 808 nm-NIR laser (1.5 W for 6 min) for PTT. After treatments, tumor sizes are measured for 2 weeks (tumor volume=$W^2 \times L/2$, W=width, L=length).

3.3 Result and Discussion

3.3.1 Synthesis of theranostic NPs

Theranostic NPs provide cancer diagnosis and targeted therapies (**Figure 3.1**). The detailed synthetic procedures and characterizations are described in **Figure 3.2** and experimental section. The corresponding TEM images of each step are provided in **Figure 3.3**. These NPs consist of Au nanorod (NR) core coated with mesoporous silica shell (MSS) to create a photothermally active core-shell structure (Au NR@MSS), on which fluorescence dye (rhodamine B), PDT dye, and Dox are loaded. PNIPAAm is polymerized on the surface of MSS to provide the effective encapsulation of Dox.

The hydrodynamic size of NPs is shown in the TEM images and in the dynamic light scattering measurement data at room temperature (**Figure 3.4a**). Au NRs are characterized by the absorption peaks at 540 nm (transversal) and 800 nm (longitudinal) in the UV-visible spectrometry measurement (**Figure 3.4b**). The longer wavelength of longitudinal absorption (relative to transverse) is due to the aspect ratio (~4) of the nanorod (8 × 30 nm). Since 800 nm wavelength is the optical window

(the wavelength region of the high penetration depth) of our body, a NIR laser can hyperthermally activate Au NRs. The surface area of the synthesized MSS on Au NRs is sufficiently large (BET data in **Figure 3.4c**) to load FL dyes, PDT dyes and chemo-drugs (Dox). The amount of drugs loaded and PDT dyes (Chlorine 6) conjugated on NPs are 0.86 g Dox per g Au and 0.06 g PDT dye per g Au, respectively, which are measured by using UV-vis spectrophotometer and ICP-AES. Several different concentrations of NPs for the uptake into HT-29 cancer cells are used for the ICP-MS analysis to identify the amount of NPs (Au mg per cell), which is necessary to identify for effective phototherapy. The results show that more than 250 NPs per one HT-29 cancer cell are needed to treat the cancer cells. Florescence correlation spectroscopy (FCS) data confirm that FL dyes are well conjugated on the surface of MSS (10 FL dyes per NP) (**Figure 3.4d**). PNIPAAm is thermo-sensitive to volume change, with a critical temperature near the body temperature (36.5 °C), Dox can be inadvertently released into other organs at body temperature. Therefore, the critical temperature of the volume change is modified by making block-copolymers from N-isopropylacrylamide and acrylic acid monomers. This modification of PNIPAAm increases the critical volume change temperature from 33 °C to >35 °C. The outer

polymer layer is functionalized with a hetero-functionalized PEG (acrylate-PEG-NHS) to allow the conjugation with antibodies for the active targeting.

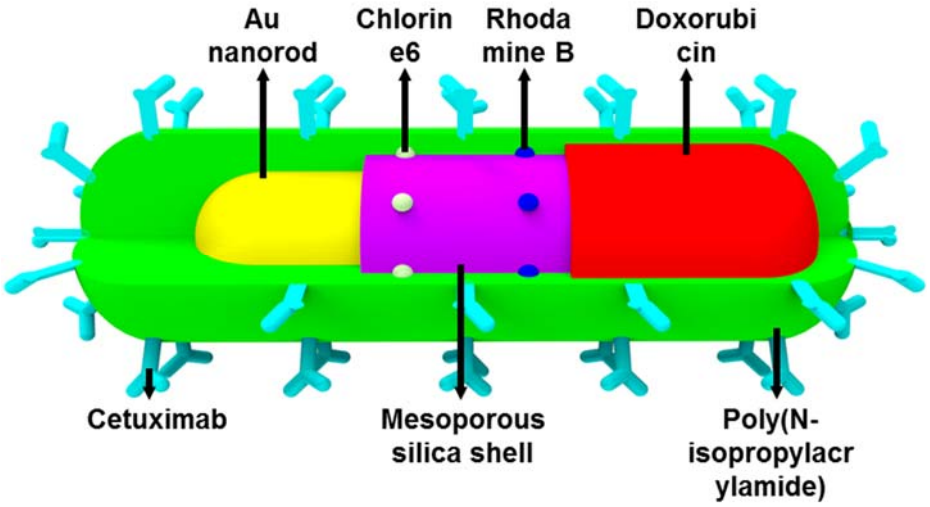

Figure 3.1. Detailed schematic illustrations of theranostic NPs.

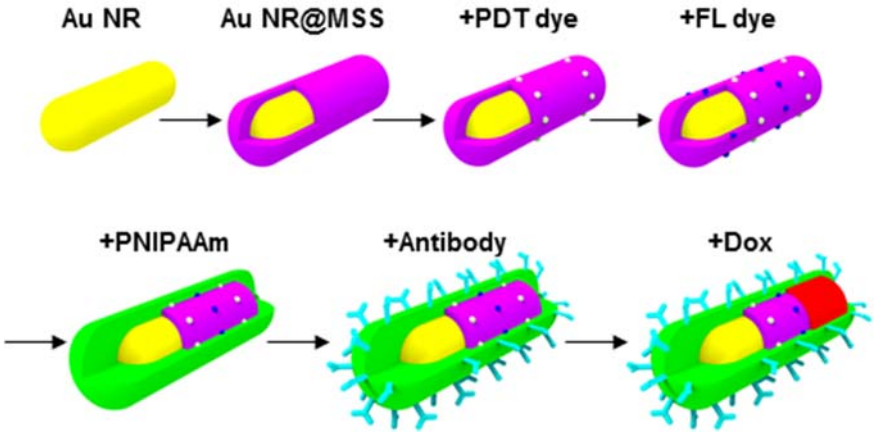

Figure 3.2. Schematic illustrations of the synthesis process of multifunctional theranostic NPs.

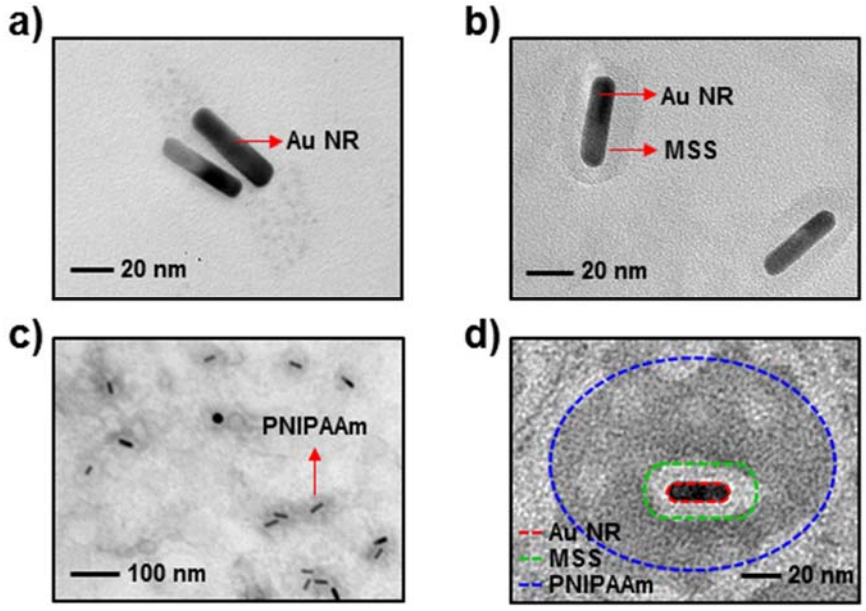

Figure 3.3. TEM images of the synthesis process of multifunctional theranostic NPs. (a) Au nanorod. (b) Au NR@meso-porous silica shells. (c) Au NR@MSS@PNIPAAm. (d) Magnified TEM image of theranostic NP.

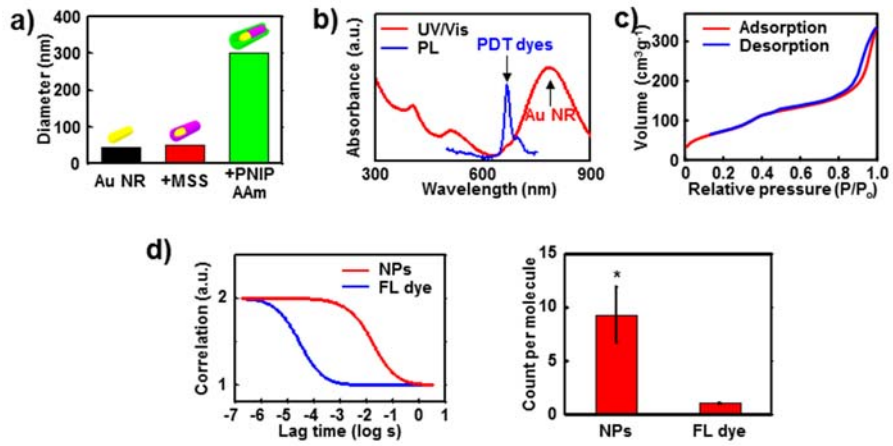

Figure 3.4. Characterization of multifunctional theranostic NPs. (a) Hydrodynamic diameters measured by the dynamic light scattering at room temperature. (b) Ultraviolet-visible absorption and photoluminescence spectroscopy data of Au NR@MSS@PDT dye. Characteristic absorption peaks for Au NR (PTT) and PDT dyes are shown. (c) BET (Brunauer-Emmett-Teller) characterization result for the estimation of the surface area of Au NR@MSS. (d) Florescence correlation spectroscopy data of NPs and FL dyes. Conjugation of fluorescent dyes on NPs is shown by correlation curve (left) and normalized count per molecule (right) (*$p < 0.01$, Student's t-test)..

3.3.2 *In-vitro* imaging and therapies by theranostic nanoparticles

Cytotoxicity tests show that these drug-loaded NPs have minimal effect on the cell viability after the PNIPAAm encapsulation in comparison with control experiments (**Figure 3.5**). The cell TEM images in **Figure 3.6** show the targeted uptake of NPs by cancer cells, which is corroborated by fluorescence images and flow cytometry data (**Figure 3.7**). Cetuximab (Erbitux) antibody is conjugated on PNIPAAm to allow the active targeting of epidermal growth factor receptors (EGFR) that are overexpressed in colon cancer (HT-29) cells. The conjugation of the theranostic NPs with tumor specific antibodies can distinguish the subtypes of tumor by fluorescence imaging.

These theranostic NPs can treat cancer cells via reactive oxygen species (ROS) generation, photo-induced hyperthermia, and controlled drug release. The photo-activation of NPs is localized to laser-irradiated regions and controlled by modulating the laser intensity. Direct control of the laser light, which is delivered through an optical fiber and guided with the endoscope, can overcome many issues related to the penetration depth of light. Because colon cancers are normally located in superficial regions, this system is less affected by the penetration depth problem of light in comparison with other tumor cases. PDT dyes on NPs are more

efficiently delivered to and taken up by cancer cells (**Figure 3.8a**), compared with controls (cancer cells treated by free form of PDT dyes and non-treated ones), as shown in flow cytometry results (**Figure 3.8b**). When radiated by continuous wave (CW) red laser (wavelength 670 nm), PDT dyes generate ROS (**Figures 3.8c and 3.8d**) and cell viability is decreased (**Figure 3.9**). The temperature is photothermally modulated by changing particle concentration (**Figure 3.10**), CW NIR laser intensity (wavelength 808 nm), and duration of irradiation, optimized for decreasing cancer cell viability (**Figure 3.11**). Increasing temperature causes a change in the hydrodynamic diameter of NPs from ~290 to ~110 nm by the shrinkage of PNIPAAm layer, which in turn induces the release of Dox loaded in NPs (**Figure 3.12b**). The release temperature (> 45 °C) is strategically designed to be higher than the body temperature (~36.5 °C). PNIPAAm block-copolymer suppresses drug release in the absence of laser radiation (**Figures 3.12c and 3.12d**), thus minimizing side-effects of Dox (**Figures 3.13**). Furthermore, viability tests of cancer cells after PDT, PTT, PTT/chemo- and combined therapy (using GaAs pulsed laser; wavelength 690 nm, power 30 mW for red laser and wavelength 808 nm, power 30 mW for NIR laser) confirm the synergistic effect of the combined treatment (**Figure 3.14**).

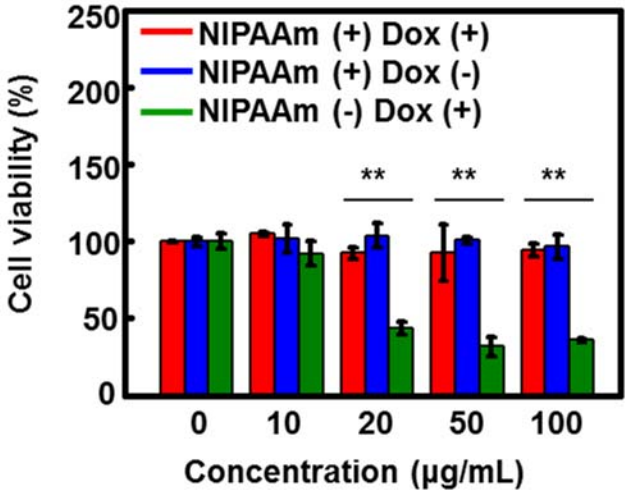

Figure 3.5. Cell viability measurement of Dox-loaded NPs with (red) and without (green) the PNIPAAm encapsulation. Another control group is Dox-unloaded NPs with PNIPAAm encapsulation (blue) (*$p <$ 0.001, Student's t-test).

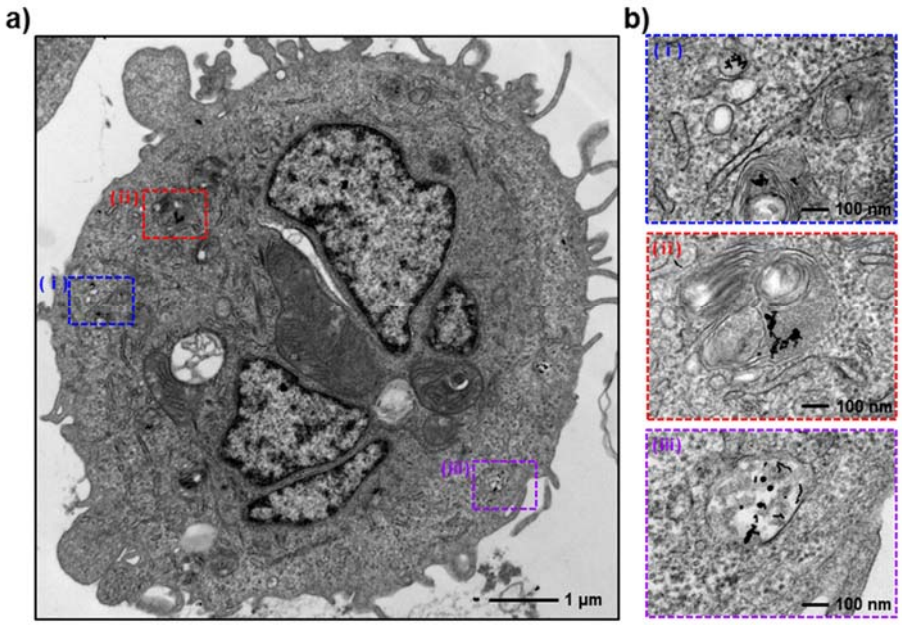

Figure 3.6. TEM observation of the cellular uptake of theranostic NPs (a) Cell TEM image of theranostic NPs uptaken by a HT-29 cancer cell at the low magnification. (b) Cell TEM images of theranostic NPs uptaken by a HT-29 cancer cell at the high magnification.

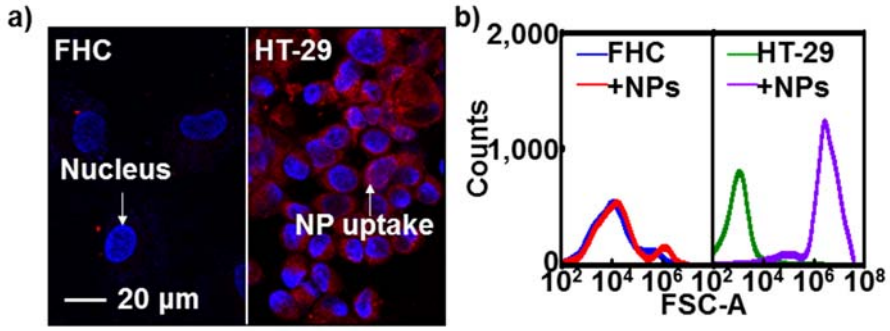

Figure 3.7. Cellular uptake of thernanostic NPs. (a) Confocal microscope images (left: normal epithelial colon cell (FHC), right: colon cancer cell (HT-29) after the active targeting). Blue fluorescence areas show 4',6-diamidino-2-phenylindole(DAPI) dyed nucleus and Red areas show rhodamine B conjugated NPs. (b) Flow cytometry data of FHC and HT-29, which show the targeted uptake of NPs to HT-29 only.

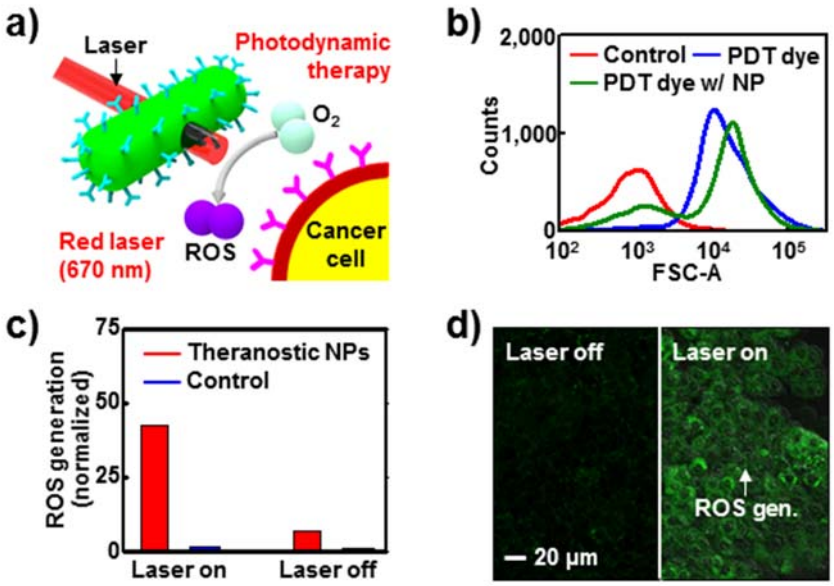

Figure 3.8. Photodynamic therapy of theranostic NPs. (a) Schematic illustration of photodynamic therapy. (b) Quantitative comparison of cellular uptake of free PDT dyes and conjugated PDT dyes on NPs by flow cytometry. (c) Measurement of the ROS generation by theranostic NPs using singlet oxygen sensor green reagent before and after CW red laser irradiation. (d) Fluorescence images of ROS generation by using DHR123 dyes before and after CW red laser radiation

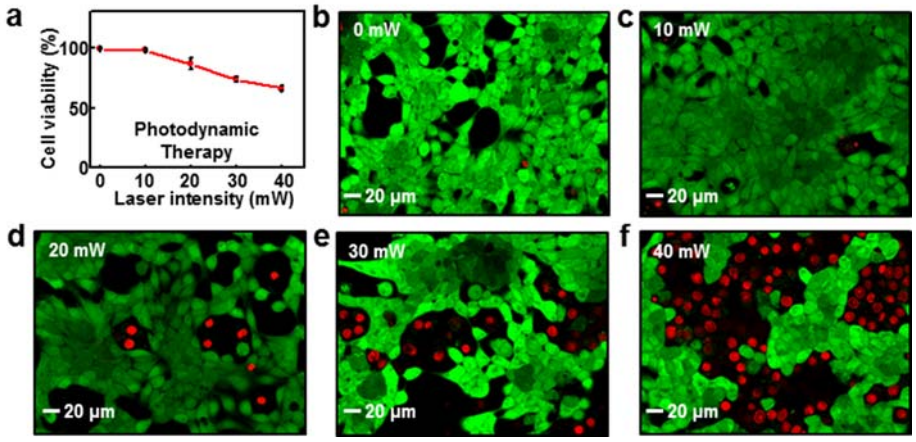

Figure 3.9. Optimization of photodynamic therapy. (a) Cell viability after photodynamic therapy. (b-f) Optimization of photodynamic therapy by modulating the power of pulsed red laser (green: live cells, red: dead cells).

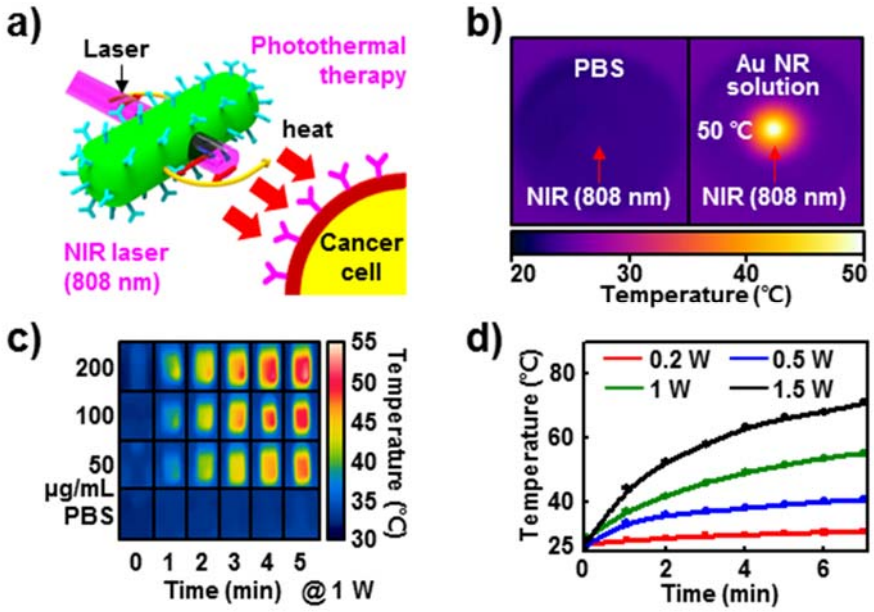

Figure 3.10. Photothermal therapy of theranostic NPs. (a) Schematic illustration of photothermal therapy. (b) Localized photothermal activation of theranostic NPs with pulsed NIR laser irradiation. (c) IR camera images of NP suspensions of different concentrations under CW NIR laser radiations of various times. (d) Relationship between the radiation time and temperature for different laser powers at the constant NP concentration of 200 μg/mL.

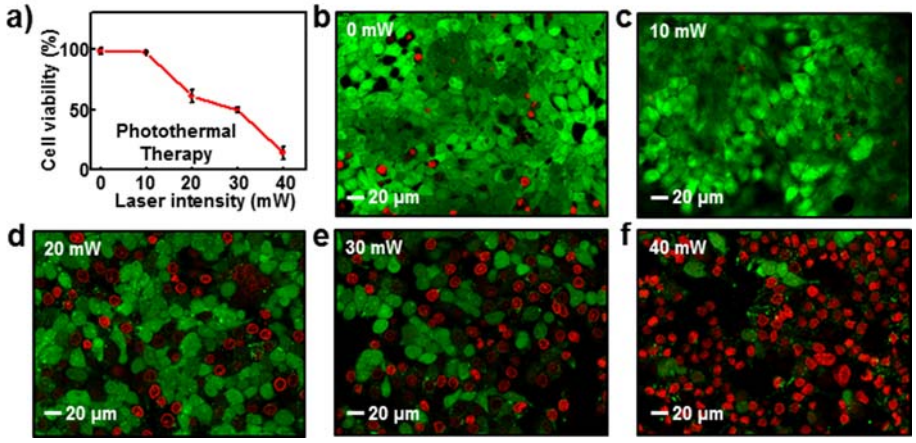

Figure 3.11. Optimization of photothermal therapy. (a) Cell viability after photothermal therapy. (b-f) Optimization of photothermal therapy by modulating the power of pulsed red laser (green: live cells, red: dead cells).

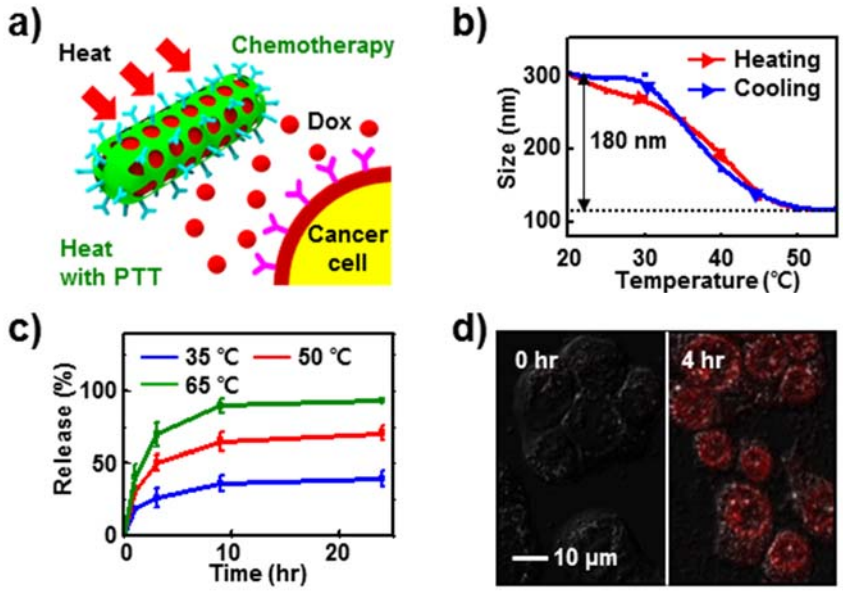

Figure 3.12. Thermo-responsive chemotherapy of theranostic NPs. (a) Schematic illustration of thermo-responsive chemotherapy. (b) Reversible change of the hydrodynamic diameter of NPs with respect to the temperature. (c) Thermally controlled drug release profiles. (d) Confocal microscope images of Dox release (left: 0 hour, right: 4 hours) from theranostic NPs treatment. Red fluorescence means Dox.

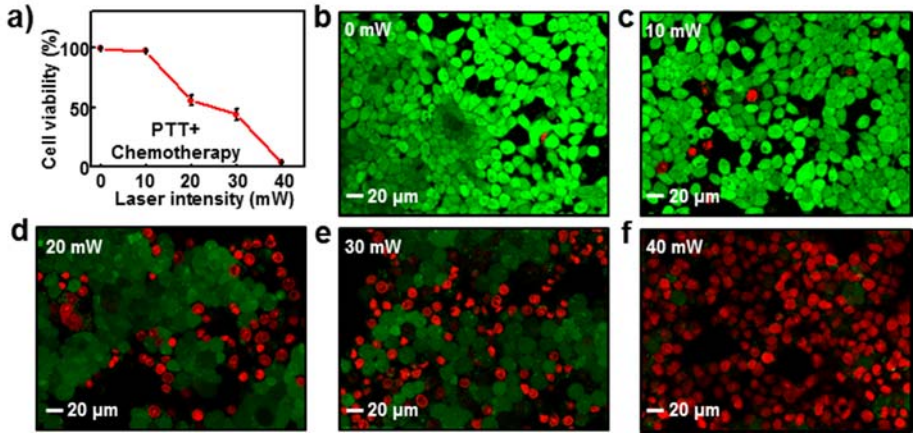

Figure 3.13. Optimization of thermo-responsive chemotherapy. (a) Cell viability after chemotherapy. (b-f) Optimization of chemotherapy by modulating the power of pulsed red laser (green: live cells, red: dead cells).

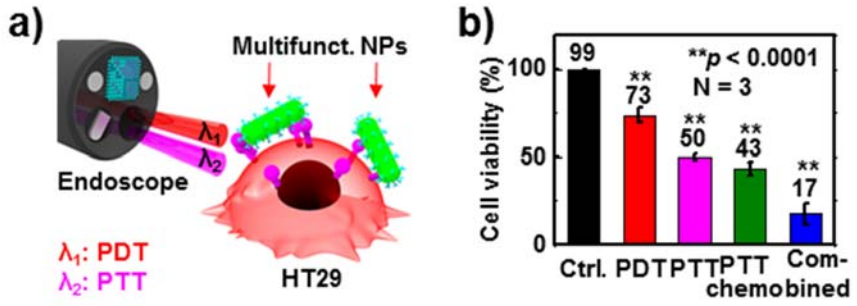

Figure 3.14. Synergetic effect of combined therapies under pulsed laser irradiation. (a) Schematic illustration of the endoscope-guided phototherapy. (b) Cell viability after various therapies (**$p < 0.0001$, Student's t-test).

3.3.3 *In-vivo* nanoparticle targeting of colon cancer

The integrated system, transparent electronics on the endoscope and theranostic NPs actuated by guided lasers, can be applied to *in-vivo* models (**Figure 3.15**). Endoscopic treatment of colon cancer (HT-29) grown on the sub-dermis surface of BALB/c-nude mouse begins with the injection of NPs intravenously through the tail vein. Since colon cancer models are not available in large animals and endoscopes are too large for gastrointestinal tracts of small animals, we conduct *in-vivo* studies using mouse subcutaneous colon cancer models. Side effects from Dox are minimized, however, since the release of Dox loaded on NPs is suppressed by the PNIPAAm encapsulation. Fluorescence image of resected organs and biodistribution analysis data show successful targeting (**Figures 3.16a and 3.16b**). Most NPs are cleared from the blood in 1 day due to the short circulation time ($t_{1/2}$ = 20 min; **Figure 3.16c**). A large number of NPs are delivered to the tumor within 6 hours of injection and accumulate in the tumor for 24 hours (**Figure 3.17**). Active targeting using the antibody conjugation shows enhancement in the targeting efficiency of NPs (**Figure 3.18**).

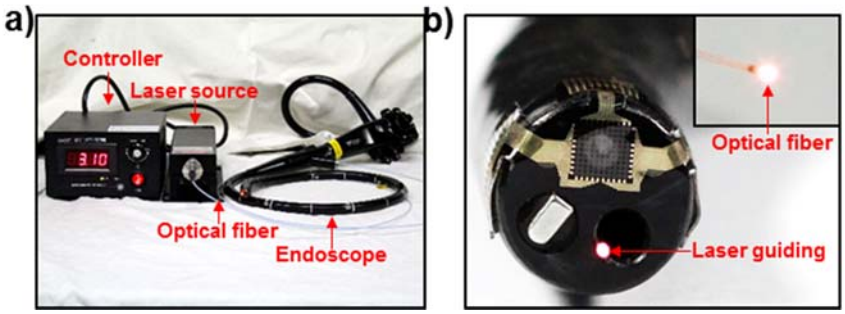

Figure 3.15. Laser guiding system through the instrumented surgical endoscope. (a) Image of the laser guiding system through the endoscope using the optical fiber. (b) Optical-fiber-guided laser irradiation through the endoscope. Inset shows the magnified view of the laser from the optical fiber tip.

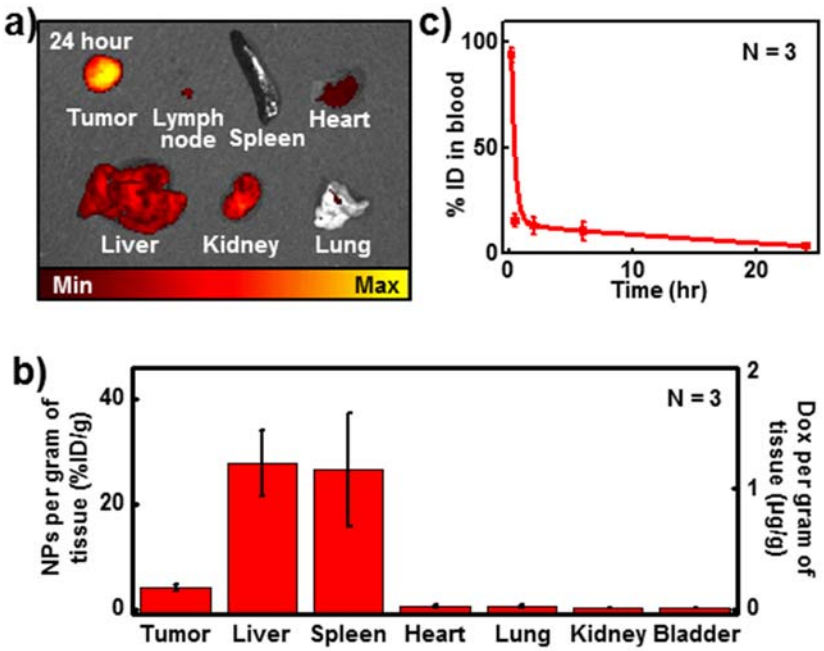

Figure 3.16. *In vivo* analysis of biodistribution and pharmakokinetics of theranostic NPs. (a) IVIS *ex-vivo* organ images after 6 hours from the IV injection of NPs. (b) ICP-MS analysis data that show the bio-distribution of NPs after 24 hours from the IV injection (left axis: biodistribution data of theranostic NPs in each organ based on the percentage of injected dose per gram tissue, right axis: biodistribution data of drug in each organ) (mouse number = 3). (c) Pharmacokinetic data for theranostic NPs in the mouse model ($t_{1/2}$ = 20 min) (mouse number = 3).

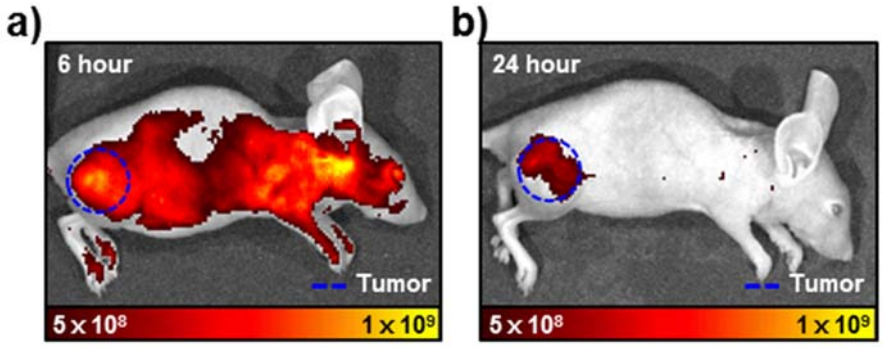

Figure 3.17. IVIS whole body images after intravenous injection of theranostic NPs (a) 6 hours (b) 24 hours.

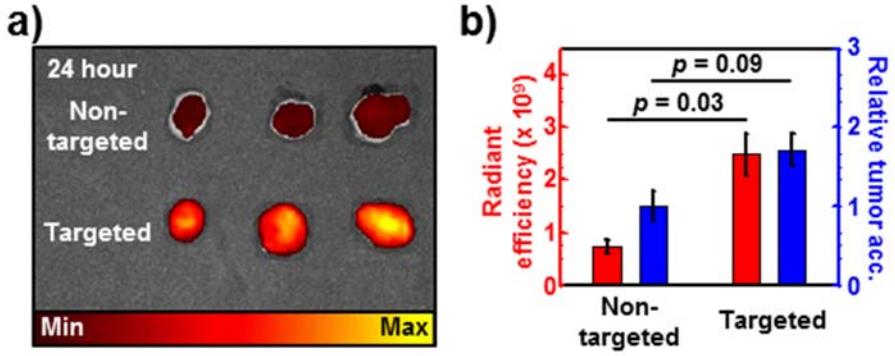

Figure 3.18. *In vivo* analysis of the active targeting. (a) IVIS *ex-vivo* tumor images of non-targeted and targeted NPs after 24 hours from the intravenous injection (mouse number is three for each experimental group). (b) ROI (region of interest) values in IVIS *ex-vivo* tumor images of **Figure 3.18a** (p = 0.03, Student's t-test) and corresponding normalized ICP-MS analysis data by the amount of theranostic NPs in non-targeted tumors (p = 0.09, Student's t-test) (mouse number is three for each experimental group).

3.3.4 *In-vivo* nanoparticle-based colon cancer treatment

Cancer cells are treated with theranostic NPs that are locally activated using CW red and NIR lasers to induce PDT (ROS), PTT (heat) and chemotherapy (Dox). The effectiveness of these multiple interventions is confirmed *in-vivo* by tracking changes in tumor volume (HT-29) based on visual observations (**Figure 3.19**). Tumor volume increases in the control group (no therapy) after 2 weeks, whereas it decreases in the treated groups (**Figure 3.20**). Furthermore, when the tumor grown on the mouse model is either laser-irradiated without injecting NPs or treated with chemo-drugs (Dox) only without targeting carriers (NPs), the tumor volume increases (**Figure 3.21**). The combined therapy group (PDT, PTT, and chemo-therapy all together) exhibits dramatic decrease in the tumor volume. Since the PTT+chemo therapy already has a good therapeutic effect and suppresses the tumor growth in our *in-vivo* model, this makes little difference in tumor volume between PTT+chemo and combined therapies. However, the combined therapy shows its higher effectiveness than other therapies in the *in-vitro* test (**Figure 3.14**). The hematoxylin and eosin (H&E) staining and terminal deoxynucleotidyl transferase dUTP nick and labeling (TUNEL) assay images of the tumor after treatments reveal irregular structures due to both apoptosis and necrosis

of cancer cells (**Figure 3.22**). From 4',6-diamidino-2-phenylindole (DAPI) and cleaved caspase-3 staining images, it is assumed that cell death is caused by apoptosis (**Figure 3.23**). And organ H&E assay shows that theranostic nanoparticles are non-toxic to mouse model (**Figure 3.24**). Although further large animal studies are required, the translation of theranostic nanoparticles for human patients can be pursued.

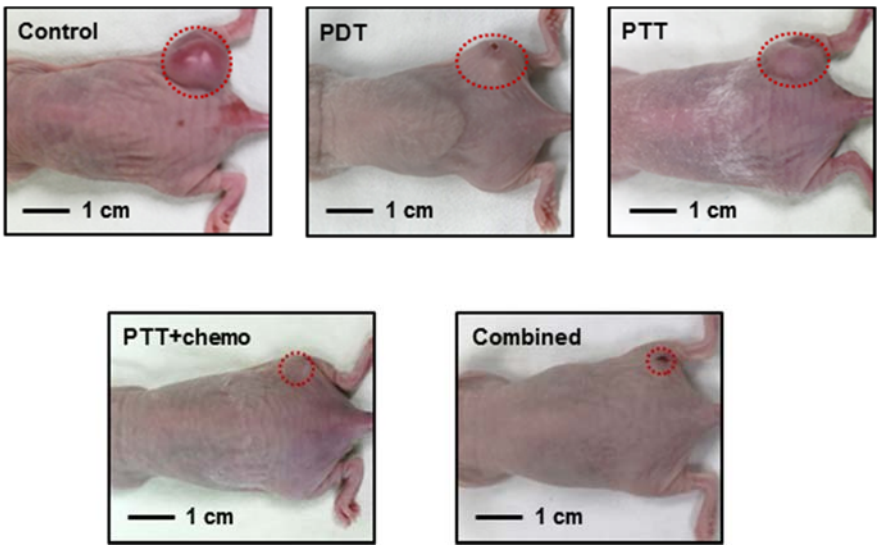

Figure 3.19. Optical images of the mouse model with HT-29 tumors after multimodal treatments.

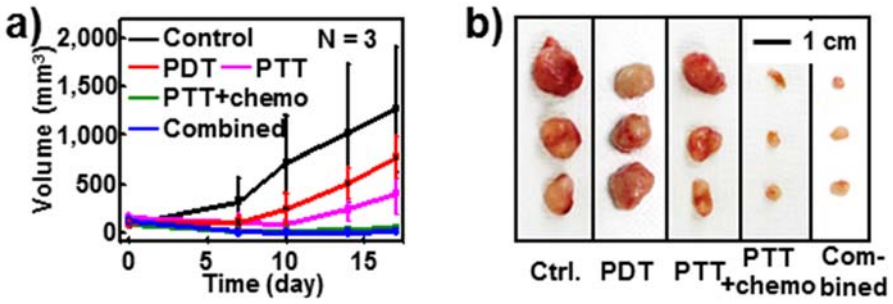

Figure 3.20. (a) Summary of tumor volume changes. (b) Corresponding tumor images of **Figure 3.20a** (mouse number = 3 for each).

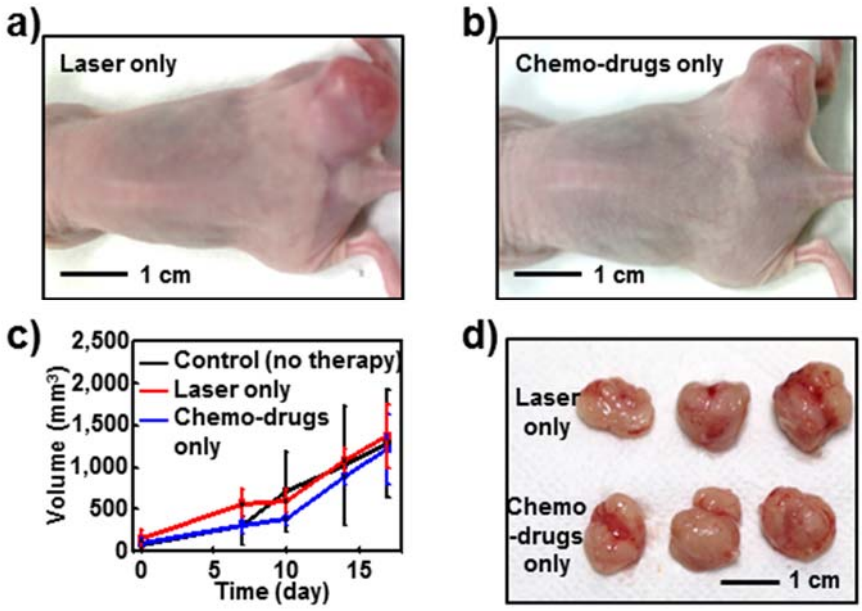

Figure 3.21. *In vivo* tumor treatments without theranostic NPs. Images of the mouse model with HT-29 tumors (a) after 808 nm laser irradiation only, (b) after chemo-drugs (Dox) therapy only. Two treated groups without theranostic NPs show the tumor growth. (c) Summary of tumor volume changes of **Figures 3.21a and 21b** with the control group (mouse number is three for each experimental group). (d) Extracted tumor images after treatments (up: 808 nm laser irradiation only, bottom: chemo-drugs therapy

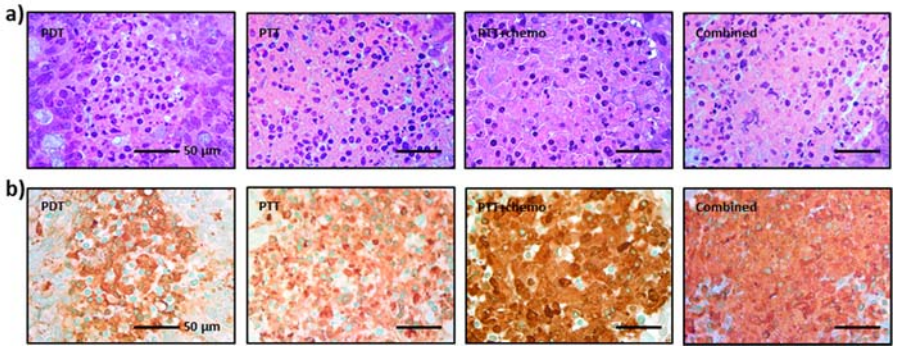

Figure 3.22. H&E and TUNEL assay after photo-therapies using theranostic NPs *in vivo* (a) Hematoxylin and eosin (H&E) staining images of HT-29 tumor tissues after PDT, PTT, PTT+chemo and combined therapy. (b) TUNEL assay images of HT-29 tumor tissues after PDT, PTT, PTT+chemo and combined therapy.

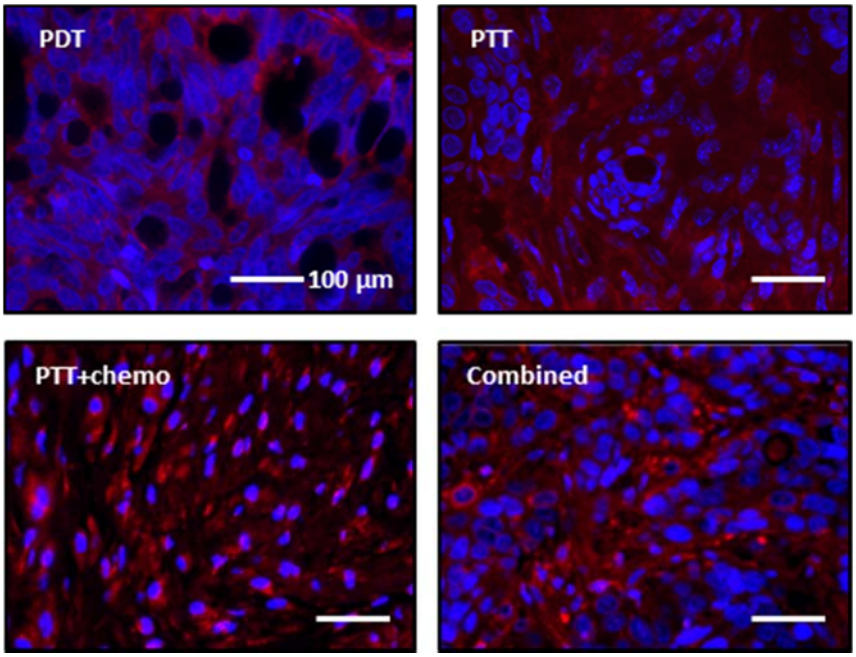

Figure 3.23. DAPI and cleaved caspase-3 staining of HT-29 tissues after PDT, PTT, PTT+chemo, and combined therapy

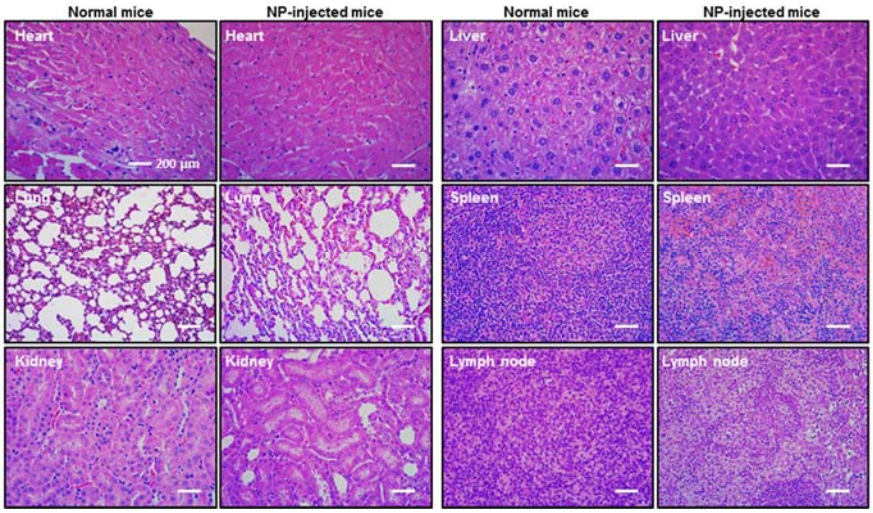

Figure 3.24. *In vivo* nanoparticle toxicity. Hematoxylin and eosin (H&E) stained tissue images from various organs of normal and NP-injected mouse.

3.4 Conclusion

In this chapter, theranostic nanoparticles for minimally invasive endoscopic surgery are described. *In-vitro* and *in-vivo* experiments show that these nanoparticles can provide fluorescent mapping and combined therapies (photothermal-, photodynamic-, and chemo- therapy) for the diagnosis and treatment of colon cancer. These nanoparticles can also simplify the diagnostic process of endoscopic surgery and enhance the accuracy of the diagnosis, using simultaneous fluorescent imaging. Moreover, the combined therapies have synergetic effects for the treatment of colon cancer cells *in-vitro* and *in-vivo*. Therefore, the developed nanoparticles can provide an assistive tool for endoscopic surgery of colon cancers.

Most of the contents of this chapter were published in the article, "An Endoscope with Integrated Transparent Bioelectronics and Theranostic Nanoparticles for Colon Cancer Treatment." (*Nature Communications* **2015, *6*, 10059)

3.5 References

[1] Kim, J.; Piao, Y.; Hyeon, T. *Chem. Soc. Rev.* **2009**, *38,* 372.

[2] Burns, A.; Ow, H.; Wiesner, U. *Chem. Soc. Rev.* **2006**, *35*, 1028.

[3] Phillips, E.; Penate-Medina, O.; Zanzonico, P. B.; Carvajal, R. D.; Mohan, P.; Ye, Y.; Humm, J.; Gönen, M.; Kalaigian, H.; Schöder, H.; Strauss, H. W.; Larson, S. M.; Wiesner, U.; Bradbury, M. S. *Sci. Transl. Med.* **2014**, *6*, 260ra149.

[4] Petros, R. A.; DeSimone, J. M. *Nat. Rev. Drug Discov.* **2010**, *9*, 615.

[5] Vivero-Escoto, J. L.; Huxford-Phillips, R. C.; Lin, W. *Chem. Soc. Rev.* **2012**, *41*, 2673.

[6] Lee, J.-H.; Huh, Y.-M.; Jun, Y.-W.; Seo, J.-W.; Jang, J.-T.; Song, H.-T.; Kim, S.; Cho, E.-J.; Yoon, H.-G.; Suh, J.-S.; Cheon, J. *Nat. Med.* **2007**, *13*, 95.

[7] Kim, S.; Lim, Y. T.; Soltesz, E. G.; De Grand, A. M.; Lee, J.; Nakayama, A. ; Parker, J. A.; Mihaljevic, T.; Laurence, R. G.; Dor, D. M.; Cohn, L. H.; Bawendi. M. G.; Frangioni, J. V. *Nat. Biotechnol*. **2003**, *22*, 93.

[8] Singh, N.; Karambelkar, A.; Gu, L.; Lin, K.; Miller, J. S.; Chen, C. S.; Sailor, M. J.; Bhatia, S. N.. *J. Am. Chem. Soc.* **2011**, *133*, 19582.

[9] Ling, D.; Park, W.; Park, S.-J.; Lu, Y.; Kim, K. S.; Hackett, M. J.; Kim, B. H.; Yim, H.; Jeon, Y. S.; Na, K.; Hyeon, T. *J. Am. Chem. Soc.* **2014**, *136*,

5647.

[10] Yavuz, M. S.; Cheng. Y.; Chen, J.; Cobley, C. M.; Zhang, Q.; Rycenga, M.; Xie, J.; Kim, C.; Song, K. H.; Schwartz, A. G.; Wang, L. V.; Xia, Y. *Nat. Mater.* **2009**, *8*, 935.

[11] Idris, N. M.; Gnanasammandhan, M. K.; Zhang, J.; Ho, P. C.; Mahendran, R.; Zhang, Y. *Nat. Med.* **2012**, *18*, 1580.

[12] Liu, H.; Chen, D.; Li, L.; Liu, T.; Tan, L.; Wu, X.; Tang, F. *Angew. Chem. Int. Ed.* **2011**, *50*, 891.

[13] Garai, E.; Sensarn, S.; Zavaleta, C. L.; Loewke, N. O.; Roqalla, S.; Mandella, M. J.; Felt, S.; Jana, N. R.; Gearheart, L.; Murphy, C. J. *J. Phys. Chem. B.* **2001**, *105*, 4065.

[14] Zhang, Z.; Wang, J.; Nie, X.; Wen, T.; Ji, Y.; Wu, X.; Zhao, Y.; Chen. C. *J. Am. Chem. Soc.* **2014**, *136*, 7317.

[15] Kudo, S.; Kashida, H.; Tamura, T.; Koqure. E; Imai. Y.; Yamano, H.; Hart, A. R. *World J. Surg.* **2000**, *24*, 1081.

[16] Garai, E.; Sensarn, S.; Zavaleta, C. L.; Loewke, N. O.; Roqalla, S.; Mandella, M. J.; Felt, S. A.; Friedlan, S.; Liu, J. T.; Gambhir, S. S.; Contaq, C. H. *PLOS One* **2015**, *10*, e0123185.

[17] Tennant, D. A.; Duran, R. V.; Gottlieb E. *Nat. Rev. Cancer* **2010**, *10*, 267.

[18] Vanneman, M.; Dranoff, G. *Nat. Rev. Cancer* **2012**, *12*, 237.

[19] Zhang, K. ; Hao, L.; Hurst, S. J. ; Mirkin, C. A. *J. Am. Chem. Soc.* **2012**, *134*, 16488.

[20] Adams, G. P.; Weiner, L. M. *Nat. Biotechnol.* **2005**, 23, 1147.

Bibliography

1. Journal Publication

1) Hyunjae Lee, **Changyeong Song** (*co-first author*), Seungmin Baik, Dokyoon Kim, Taeghwan Hyeon, Dae-Hyeong Kim

"Device-assisted transdermal drug delivery."

Advanced Drug Delivery Reviews, **2017**, *submitted*

2) Hyunjae Lee, **Changyeong Song** (*co-first author*), Yong Seok Hong, Min Sung Kim, Hye Rim Cho, Taegyu Kang, Kwangsoo Shin, Seung Hong Choi, Taeghwan Hyeon, Dae-Hyeong Kim

"Wearable/disopasable sweat-based glucose monitoring device with multi-stage transdermal drug delivery module."

Science Advances, **2017**, 3, e1601314

3) Hyunjae Lee, Youngsik Lee, **Changyeong Song** (*co-first author*), Hye Rim Cho, Roozbeh Ghaffari, Tae Kyu Choi, Kyung Hoon Kim, Young

Bum Lee, Daishun Ling, Hyuk Lee, Su Jong Yu, Seung Hong Choi, Taeghwan Hyeon, Dae-Hyeong Kim

"An endoscope with integrated transparent bioelectronics and theranostic nanoparticles for colon cancer treatment."

Nature Communications, **2015**, 6, 10059

4) Min Soh, Dong-Wan Kang, Han-Gil Jeong, Dokyoon Kim, Do Yeon Kim, Wookjin Yang, **Changyeong Song**, Seungmin Baik, In-Young Choi, Seul-Ki Ki, Hyek Jin Kwon, Taeho Kim, Chi Kyung Kim, Seung-Hoon Lee, Taeghwan Hyeon

"Ceria-zirconia nanoparticles as an enhanced multi-antioxidant for sepsis treatment."

Angewandte Chemie Internatinal Edition, **2017**, ASAP

5) Jaemin Kim, Donghee Son, Mincheol Lee, **Changyeong Song**, Jun-Kyul Song, Ja Hoon Koo, Dong Jun Lee, Hyung Joon Shim, Ji Hoon Kim, Minbaek Lee, Taeghwan Hyeon, Dae-Hyeong Kim

"A wearable multiplexed silicon nonvolatile memory array using nanocrystal charge confinement."

Science Advances, **2016**, 2, e1501101

6) Suji Choi, Jinkyung Park, Wonji Hyun, Jangwon Kim, Jaemin Kim, Young Bum Lee, **Changyeong Song**, Hye Jin Hwang, Ji Hoon Kim, Taeghwan Hyeon, Dae-Hyeong Kim

"Stretchable heater using ligand-exchanged silver nanowire nanocomposite for wearable articular thermotherapy."

ACS Nano, **2015**, *9*, 6626-6633

7) Donghee Son, Jongha Lee, Shutao Qiao, Roozbeh Ghaffari, Jaemin Kim, Ji Eun Lee, **Changyeong Song**, Seok Joo Kim, Dong Jun Lee, Samuel Woojoo Jun, Shixuan Yang, Minjoon Park, Jiho Shin, Kyungsik Do, Mincheol Lee, Kwanghun Kang, Cheol Seong Hwang, Nanshu Lu, Taeghwan Hyeon, Dae-Hyeong Kim

"Multifunctional wearable devices for diagnosis and therapy of movement disorders"

Nature Nanotechnology, **2014**, 9, 397-404

8) Daishun Ling, Hongping Xia, Wooram Park, Michael J. Hackett,

Changyeong Song, Kun Na, Kam Man Hui, Taeghwan Hyeon

"pH-sensitive nanoformulated triptolide as a targeted therapeutic strategy for hepatocellular carcinoma"

ACS Nano, **2014**, 8, 8027-8039

9) Daishun Ling, Wooram Park, Yong Il Park, Nohyun Lee, Fangyuan Li, **Changyeong Song**, Su-Geun Yang, Seung Hong Choi, Kun Na, Taeghwan Hyeon

"Multiple-Interaction Ligands Inspired by Mussel Adhesive Protein: Synthesis of Highly Stable and Biocompatible Nanoparticles"

Angewandte Chemie International Edition, **2011**, 50, 11360-11365

2. International Conference Presentation

1) **Changyeong Song**, Hyunjae Lee, Youngsik Lee, Dae-Hyeong Kim, Taeghwan Hyeon

"Multifunctional Endoscope System with Theranostic Nanoparticles and Bio-electronics for Colon Cancer Treatment"

2016 MRS Fall Meeting & Exhibit, BOSTON, USA, November 27-

December 2, 2016

2) **Changyeong Song**, Hyunjae Lee, Dae-Hyeong Kim, Taeghwan Hyeon

"Theranostic Nanoparticles and Transparent Bio-electronics for Endoscope-based Cancer Treatment"

17th Korea-Japan Joint Symposium on Organometallic and Coordination Chemistry, Busan, Korea, November 3-5, 2016

3) **Changyeong Song**, Hyunjae Lee, Dae-Hyeong Kim, Taeghwan Hyeon

"Theranostic Nanoparticles with Bio-electronics for Endoscope-based Colon Cancer Treatment"

20th International Vacuum Congress, Busan, Korea, August 21-26, 2016

4) Hyunjae Lee, **Changyeong Song**, Taeghwan Hyeon, Dae-Hyeong Kim

"An Endoscope with Integrated Transparent Bioelectronics and Theranostic Nanoparticles for Colon Cancer Treatment"

The 9th International Conference on Quantum Dots, Jeju, Korea, May 22-27, 2016

5) **Changyeong Song**, Taeghwan Hyeon,

"Theranostic Nanoparticles with TransparentBio-electronics for Endoscope-based Colon Cancer Treatment"

IUMRS-ICAM 2015, Jeju, Korea, October 25-29, 2015

3. Award

Best Poster Award at IUMRS-ICAM 2015

IUMRS-ICAM 2015, Jeju, Korea, October 25-29, 2015

초 록

최근 나노입자를 이용한 진단 및 치료를 포함한 생의학적 연구가 활발히 진행되고 있다. 내부 혹은 외부 자극에 의해 약물 전달이 조절 되는 시스템은 목표로 하는 부위에 선택적으로 치료 효과를 낼 수 있다는 데 장점이 있다. 다양한 자극 민감성 약물 전달 중, 온도 민감성 약물 전달 시스템은 열적 자극을 조절함에 따라 on/off 약물 전달 및 단계적 약물 전달이 가능하다. 또한, 유연소자와의 결합을 통해 온도 민감성 약물 전달 시스템은 정밀한 온도 조절, 다단계 약물 전달, 무선 약물 전달 등 괄목할 성장을 할 수 있을 것으로 예상된다.

먼저, 상 변화 물질을 기존 미세침 시스템에 도입함으로써 온도 민감성 미세침을 제작하였다. 상 변화 물질을 약물 전달체로 사용하기 위해, 침을 이용한 초음파 기법을 통해 상 변화 나노입자를 성공적으로 합성하였다. 서로 다른 상 변화 물질을 사용하여, 약물 배출 온도를 40, 45 °C로 조절하였다. 합성된 상 변화 나노입자는 2형 당뇨약인 메트폴민을 담지한

후, 녹는점 이상으로 열이 가해질 때에만 약물을 전달하였다. 세 개의 경로를 가지는 히터와 온도 센서와 결합하여, 미세침은 당뇨 치료를 위한 최대 여섯 단계의 다단계 약물전달이 가능하였다.

다음으로 대장암 치료를 위한 온도 민감성 고분자로 둘러쌓인 광학 및 화학 약물이 포함된 치료 및 진단이 가능한 나노입자를 개발하였다. 대장암 치료에 사용하는 내시경과 결합하여, 레이저의 투과 깊이 문제를 극복할 수 있었다. 개발된 나노입자의 골드 나노라드는 적외선 영역의 빛을 조사하였을 시, 광열 치료 및 화학 약물(독소루비신)의 온도 민감성 전달에 사용되는 열을 발생시켰다. 또한, 다공성의 실리카 셸에 있는 광역학 염료는 붉은 레이져에 반응하여 이미징 및 광역학 치료가 가능하였다. 이러한 결합 치료(광열, 광역학, 화학)는 세포 및 쥐 실험을 통해 대장암 치료에 상승효과가 있음을 알 수 있었다. 위 나노입자는 항체와 결합하여 대장암 세포에 선택적으로 전달되며, 레이저를 이용해 나노입자가 전달된 세포만 죽임으로써 암 치료의 부작용을 최소화할 수 있을 것으로 예상된다.

주요어: 나노입자, 열 민감성, 유연소자, 약물전달, 미세침,

나노바이오기술, 생물학적 응용

학번: 2011-22920